

Initial Results of the Relative Humidity Observations by MEDA Instrument Onboard the Mars 2020 Perseverance Rover

Special Section:

The Mars Perseverance Rover
Jezero Crater Floor Campaign

Key Points:

- Humidity observations in Mars by M2020 Perseverance rover during the first 410 sols of operation are shown and discussed
- Humidity sensor MEDA-HS operations and sensor accuracy are explained
- Adsorptive single column model is tested and compared with humidity observations

Supporting Information:

Supporting Information may be found in the online version of this article.














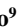




Correspondence to:

J. Polkko,
jouni.polkko@fmi.fi

Citation:

Polkko, J., Hieta, M., Harri, A.-M., Tamppari, L., Martínez, G., Viúdez-Moreiras, D., et al. (2023). Initial results of the relative humidity observations by MEDA instrument onboard the Mars 2020 Perseverance Rover. *Journal of Geophysical Research: Planets*, 128, e2022JE007447. <https://doi.org/10.1029/2022JE007447>

Received 29 JUN 2022
Accepted 12 JAN 2023

J. Polkko¹ , M. Hieta¹ , A.-M. Harri¹, L. Tamppari² , G. Martínez^{3,4}, D. Viúdez-Moreiras⁵ , H. Savijärvi⁶ , P. Conrad⁷, M. P. Zorzano Mier⁵, M. De La Torre Juarez² , R. Hueso⁸ , A. Manguira⁸ , J. Leino¹ , F. Gómez⁵ , I. Jaakonaho¹ , E. Fischer⁴ , M. Genzer¹, V. Apestigue⁹ , I. Arruego⁹ , D. Banfield¹⁰, A. Lepinette⁵ , M. Paton¹, J. A. Rodriguez-Manfredi⁵, A. Sánchez Lavega⁸ , E. Sebastian⁵, D. Toledo⁹ , A. Vicente-Retortillo⁵ , and MEDA team

¹Finnish Meteorological Institute, Helsinki, Finland, ²Jet Propulsion Laboratory–California Institute of Technology, Pasadena, CA, USA, ³Lunar and Planetary Institute, USRA, Houston, TX, USA, ⁴University of Michigan, Ann Arbor, MI, USA, ⁵Centro de Astrobiología (INTA-CSIC), Madrid, Spain, ⁶University of Helsinki, Helsinki, Finland, ⁷Carnegie Institution for Science, Washington, DC, USA, ⁸Universidad del País Vasco UPV/EHU, Bilbao, Spain, ⁹INTA, Madrid, Spain, ¹⁰Cornell University, Ithaca, NY, USA

Abstract The Mars 2020 mission rover “Perseverance”, launched on 30 July 2020 by NASA, landed successfully 18 February 2021 at Jezero Crater, Mars (Lon. E 77.4509° Lat. N 18.4446°). The landing took place at Mars solar longitude $L_s = 5.2^\circ$, close to start of the northern spring. Perseverance's payload includes the relative humidity sensor MEDA HS (Mars Environmental Dynamics Analyzer Humidity Sensor), which operations, performance, and the first observations from sol 80 to sol 410 ($L_s 44^\circ$ – 210°) of Perseverance's operations we describe. The relative humidity measured by MEDA-HS is reliable from late night hours to few tens of minutes after sunrise when the measured humidity is greater than 2% (referenced to sensor temperature). Data delivered to the Planetary Data System include relative humidity, sensor temperature, uncertainty of relative humidity, and volume mixing ratio (VMR). VMR is calculated using the MEDA-PS pressure sensor values. According to observations, nighttime absolute humidity follows a seasonal curve in which release of water vapor from the northern cap with advancing northern spring and summer is visible. At ground level, frost conditions may have been reached a few times during this season ($L_s 44^\circ$ – 210°). Volume mixing ratio values show a declining diurnal trend from the midnight toward the morning suggesting adsorption of humidity into the ground. Observations are compared with an adsorptive single-column model, which complies with observations and confirms adsorption. The model allows estimating daytime VMR levels. Short-term subhour timescales show large temporal fluctuations in humidity, which suggest vertical and spatial advection.

Plain Language Summary The Mars 2020 mission rover “Perseverance” landed successfully on 18 February 2021 at Jezero Crater, Mars. The rover's payload includes a versatile instrument suite which includes a relative humidity sensor, whose observations for the first 410 Martian days are described here. The observations show how the lowest level of atmosphere is generally dry but still exceeding saturation is feasible because of cold nights. Sensor operations and accuracy estimates are presented. Relative humidity together with MEDA pressure and air temperature observations allow calculating absolute water vapor content of air at the sensor level at nighttime. Humidity observations are also compared with models describing water vapor adsorption and desorption into and out from soil. The results show how atmospheric humidity at the rover's site experiences large subhour variability. Humidity observations help to understand interchange of humidity between the soil and the atmosphere. Water is mandatory for life, such as on earth, thus understanding these water cycle processes better are important for evaluating possibilities of past and current habitability of Mars. Perseverance is also collecting samples which maybe returned to Earth one day. Knowledge of the conditions at the times when samples were collected maybe useful.

1. Introduction

The Mars 2020 mission rover “Perseverance,” launched on 30 July 2020 by NASA, landed successfully on 18 February 2021 at Jezero Crater, Mars (Lon. E 77.4509°, Lat. N 18.4446°) at solar longitude $L_s = 5.2^\circ$. Jezero is a 45-km wide impact crater located in the Nili Fossae region close to western edge of Isidis Planitia. It is thought

that an ancient river flowed into Jezero, forming a delta, flooding the crater and forming a lake, both of which have dried out long ago (Mangold et al., 2021).

Perseverance's science objectives include studying signatures of past habitability. It will also collect and store a set of samples for possible recovery by a later mission. To prepare for human exploration, environmental conditions are recorded by Perseverance's Mars Environmental Dynamics Analyzer (MEDA) instrument package, which is one of the rover's seven primary instruments. MEDA has a set of six sensors: Air Temperature Sensor (ATS), Pressure Sensor (PS), Radiation and Dust Sensor (RDS), Relative Humidity Sensor (HS), Thermal Infrared Sensor (TIRS), and Wind Sensor (WS) (Rodriguez-Manfredi et al., 2021). In addition to MEDA's importance to future human exploration, MEDA can be used to address environmental scientific goals, including understanding the near-surface atmosphere and its relationship to the surface over which the rover is driving. In this paper, we focus on the first results of the MEDA HS Relative Humidity Sensor.

The Relative Humidity Sensor (MEDA HS) is based on capacitive polymer sensors developed by Vaisala Oyj (Vaisala-Oyj, 2020). The MEDA HS provides nighttime in situ observations of relative humidity. During the daytime, the relative humidity drops close to 0%, below the accuracy of the sensor.

This paper describes the observations by MEDA HS of the first 410 Sols of operations of the Perseverance Rover, MEDA HS operational cycles, and the limitations of the sensor as well as some initial interpretations of those results. Section 2 describes the background of the MEDA HS and water vapor in Martian atmosphere. Section 3 gives a description of the sensor, Section 4 describes how the MEDA HS has been operated onboard Perseverance, Section 5 presents an overview of the observations, and Section 6 presents comparisons between a column water model and the observations. Conclusions and discussion are in Section 7.

2. Background

Robotic exploration of Mars has followed a strategy guided by scientific consensus on the most important goals collected and defined by Mars Exploration Program Analysis Group (MEPAG) (Banfield et al., 2020), within which understanding the behavior of water remains high priority. Water is an obligatory solvent for earth-like life as we understand it. Existence and cycles of water and water vapor on past and current Mars is of high scientific importance when investigating habitability potential and possibilities that microbiological life once existed. According to geological evidence liquid water flowed on Mars in the past, forming rivers, deltas, lakes, and possibly seas (Milton, 1973; Morris et al., 2006; Mangold et al., 2021). Present water on Mars is thought to be mainly found in three reservoirs: (a) in the polar caps and surface ice, (b) in the regolith, and (c) in the atmosphere. The surface reservoirs, that is, the polar caps and regolith hold several orders of magnitude more water than the atmosphere. Thus, if all the water of the surface reservoirs melted and spread evenly all over the planet, it would result in a layer of 20–30 m deep water (D. E. Smith et al., 1999).

Water vapor in the Mars atmosphere was first observed by Earth-based spectrometer observations in 1963 (Spinrad et al., 1963). Several ground-based observations of Martian water vapor were performed since then (e.g., Clancy et al., 1992; Encrenaz et al., 1995, 2001; Jakosky, 1985; Jakosky and Haberle, 1992; Sprague et al., 1996, 2003; and references therein). Orbital observations have also characterized the water vapor abundance in the Mars atmosphere, using data from Mariner 9 (Conrath et al., 1973), Viking orbiters (Farmer et al., 1977; Fedorova et al., 2004; Jakosky and Farmer, 1982), Mars Global Surveyor (Christensen et al., 1992; M. D. Smith, 2002, 2004; M. D. Smith et al., 2001), Mars Express (Encrenaz et al., 2005; Fedorova et al., 2006, 2021; Fouchet et al., 2007; Maltagliati et al., 2011; Sindoni et al., 2011), Mars Reconnaissance Orbiter CRISM spectrometer (M. D. Smith et al., 2009) and ExoMars Trace Gas Orbiter (Aoki et al., 2019), including its seasonal, latitudinal, and longitudinal variation and, recently, its vertical profiles in the atmosphere.

Observations indicate that the Mars atmosphere has, on average, an order of 10 μm of precipitable water (pr- μm ; the thickness of the water layer if all the water vapor of the atmosphere were to be condensed onto the surface, 1 pr- μm being thus 1 g of water per square meter). The Earth's atmosphere has a few tens of mm precipitable water, thus compared to Earth, the Martian atmosphere is extremely dry (e.g., Jakosky & Haberle, 1992). Also, strong seasonal and spatial variability has been found to date, together with interannual variations mostly related to the effect of dust storms (e.g., M. D. Smith et al., 2001), with maximum abundances, as high as 80–100 pr- μm , during the northern summer at high northern latitudes, and minima in the southern hemisphere. The southern summer produces the opposite meridional effect but with a significantly lower amplitude, reaching a maximum

water vapor abundance of about half that of the northern summer column abundance, possibly as a result of the orbit eccentricity of Mars (Clancy et al., 1996). The vertical profiles of water vapor are strongly variable and influenced by dust storms (e.g., Aoki et al., 2019; Heavens et al., 2018), when water vapor is able to reach very high altitudes. However most of the water vapor remains in the lowest few kilometers of the atmosphere under normal conditions.

In situ water vapor observations are, however, much more scarce, thus the water abundance in the near-surface atmosphere has not been well characterized. In fact, only two missions to date, Phoenix lander and Mars Science Laboratory (MSL), carried on instrumentation to measure relative humidity. Water mixing ratios were able to be inferred, together with concurrent measurements of atmospheric pressure and temperature.

The Phoenix mission landed on Mars at 68.2°N, 234.2°E in 2008 (Ls 78°–147°) and operated for more than one hundred and fifty sols (P. H. Smith et al., 2009). The thermal and electrical conductivity probe (TECP) onboard the Phoenix lander returned the first in situ relative humidity measurements (Rh) from the Martian surface (Zent et al. (2010), Zent et al. (2016), Fischer et al. (2019)). Observations showed a high Rh (even reaching water vapor saturation in the atmosphere) during the nighttime and average Rh less than 5% during the daytime, increasing to 10% late in the mission. The daytime mixing ratios were more than an order of magnitude greater than those inferred during nighttime. Complementary observations detected frost deposition on the surface, occurring in the latter half of the mission. Also, it was suggested that water vapor mixed upward by daytime turbulence and convection formed the observed water ice clouds at night that precipitated back toward the surface (Whiteway et al., 2009). However, another study indicated a marked confinement of water vapor below 2.5 km of altitude during the daytime (Tamppari & Lemmon, 2020).

The study of water vapor from the Martian surface moved forward with the arrival of MSL at Gale Crater (4.6°S, 137.5°E) in 2012. Mars Science Laboratory rover carries the Rover Environmental Monitoring Station instrument, which includes an Rh sensor (Gómez-Elvira et al., 2012). Initial results have shown a dry atmosphere, with Rh barely reaching 70% during the diurnal cycle (Harri et al., 2014; Martín-Torres et al., 2015; Martínez et al., 2016, 2017). A large seasonal cycle has been observed, with maximum values reached around the southern winter solstice during the nighttime. The diurnal cycle also shows dramatic variations, with Rh being close to zero during the daytime. However, due to the very low Rh values during the daytime, the associated water mixing ratios cannot be retrieved with accuracy.

The dramatic diurnal variation observed at both landing sites, together with previous orbital observations and modeling, strongly suggests that there is a significant regolith-atmosphere exchange mechanism on Mars, probably owing to adsorption/desorption in the regolith (e.g., Jakosky et al., 1997; McConnochie et al., 2018; Melchiorri et al., 2009; Savijärvi, Martinez, Fischer, et al., 2020; Savijärvi et al., 2015, 2019; Steele et al., 2017). In addition, the effects of a global dust storm (MY34/2018 GDS) on the humidity levels were also observed by MSL (Viúdez-Moreiras et al., 2019). The near-surface water mixing ratio suggested an overnight increase during the storm at MSL's general location and a decrease during the daytime. It was hypothesized that the combined effect of a reduction in the strength of an adsorption and desorption mechanism in the regolith and the enhanced vertical mixing at night during the storm could be driving the observed effect in the diurnal cycle assuming that the inferred water vapor abundances during the GDS are correct. Savijärvi, Martinez, Harri, and Paton (2020) proposed an additional source of water vapor to minimize the mismatch between modeling efforts and observations.

3. MEDA HS Relative Humidity Instrument

The MEDA HS relative humidity instrument (HS) consists of printed circuit board of a 63 * 15 * 1 mm size, mechanical support, electrically grounded perforated thin stainless steel cover shield, and dust filter. The dust filter is made of polytetrafluoroethylene (PTFE) sheet and has pore size 0.20 μm . PCB accommodates the Humicap[®] humidity sensor elements, housekeeping temperature sensors, housekeeping reference capacitors, and electronics based on a single application specific integrated circuit. Dimensions of the sensor are 55 * 25 * 90 mm and mass is 45 g. Power consumption is 20 mW. MEDA HS sensor testing and calibrations are described in detail in Hieta et al. (2022).

The MEDA HS is mounted onto a metallic interface box which accommodates electric connector. This box is mounted onto the rover's remote sensing mast (RSM) above the MEDA ATS ATS-2 and below the other

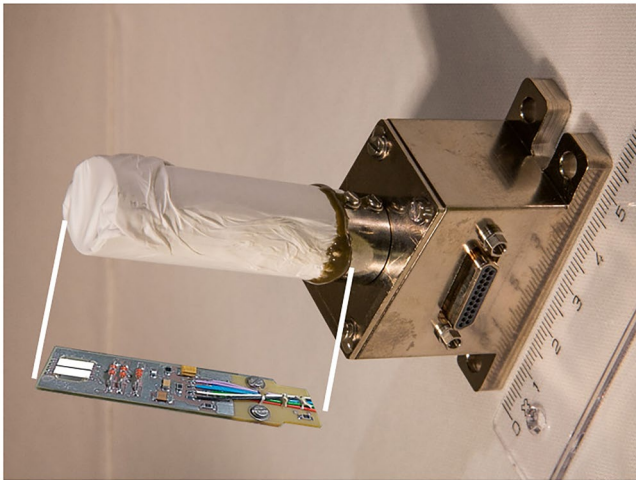


Figure 1. Meda HS (HS) relative humidity instrument. Printed circuit board (PCB) with the electronics and the Humicap® humidity sensing-elements is located inside PTFE dust filter. The PCB is accommodated by electronics on both sides.

MEDA Wind Sensor (WS). The height of the sensor above the ground is 1.50 m. The HS-sensor presented in Figures 1 and 2 shows how the sensor is mounted. The humidity sensor element also contains an integrated platinum temperature sensor, which has 1,000 Ω resistance at 0 C°, thus this resistor is called Pt1000. The relative humidity output value is referenced to this Pt1000 sensor output. The sensor element also includes a heating resistor, which is used periodically for “regenerating” the sensor. Regeneration is a heat treatment process, in which heating the sensor from ambient to +170 C° for a few minutes will clean the sensor polymer from condensed volatiles which may have contaminated the sensor. Regeneration heating has also a short term side effect. Sensor polymer membrane adsorbs and is sensitive to carbon dioxide. Regeneration heating outgasses carbon dioxide out of sensor. Adsorbing gas back takes few days and sensor readings are slightly compromised during this time.

MEDA HS works in conjunction with other sensors of the MEDA instrument suite. The atmospheric pressure data provided by the Pressure Sensor MEDA-PS are used to calculate the volume mixing ratio, VMR. MEDA Air Temperature Sensors ATS (five separate sensors), MEDA Thermal Infrared Sensor TIRS providing ground and 40 m level temperatures, and MEDA Wind Sensor WS are most useful too in analyzing MEDA-HS results.

Uncertainty analysis of the sensor was performed by consultants specialized in metrology, VTT Technical Research Centre of Finland Ltd. (VTT-Ltd., 2022) following the guidelines of the Joint Committee for Guides in Metrology (JCGM, 2008). Factors contributing to calibration uncertainty were uncertainty contributed by calibration model and nonlinearity, uncertainty of the temperature sensors (calibration of the Pt1000 sensors in the Humicap sensor elements and calibration of a reference transfer sensor used in the Pt1000 calibrations, uncertainty of the dew/frost point temperatures in the calibrations (reference hygrometers), uncertainty of the

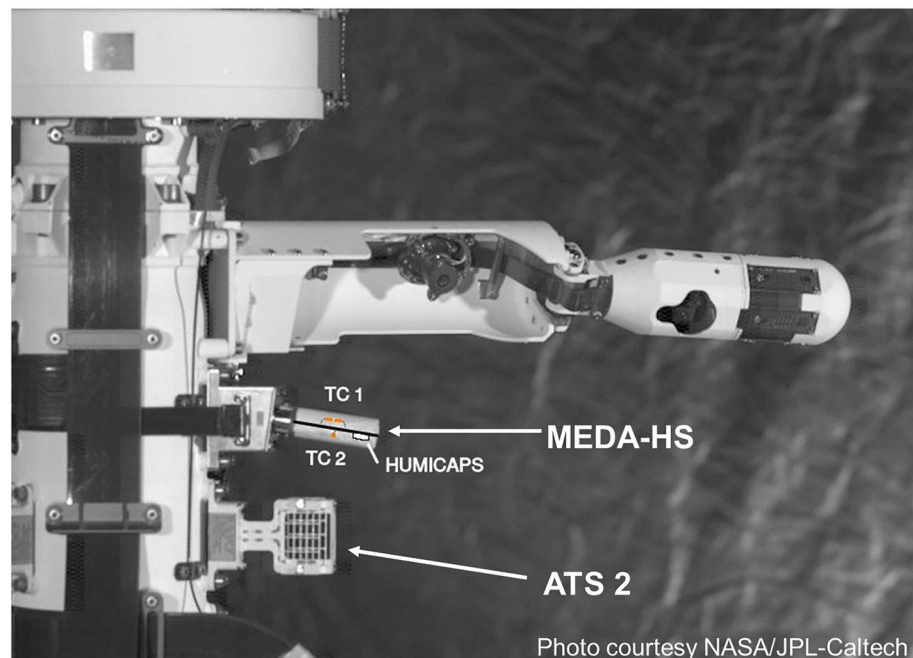


Figure 2. Meda-HS is mounted onto the remote sensing mast above ATS-2 air temperature sensor and below the Mars Environmental Dynamics Analyzer wind sensors. Height from the ground is 1.50 m. Orientation of the Meda HS circuit board is shown (inside the dust filter between TC1 and TC2 texts). The Humicap humidity sensor elements face upward (through a hole in the printed circuit board). Locations of the Termocap® 1 and 2 housekeeping T sensors TC1 and TC2 are shown. Photo NASA/JPL-Caltech.

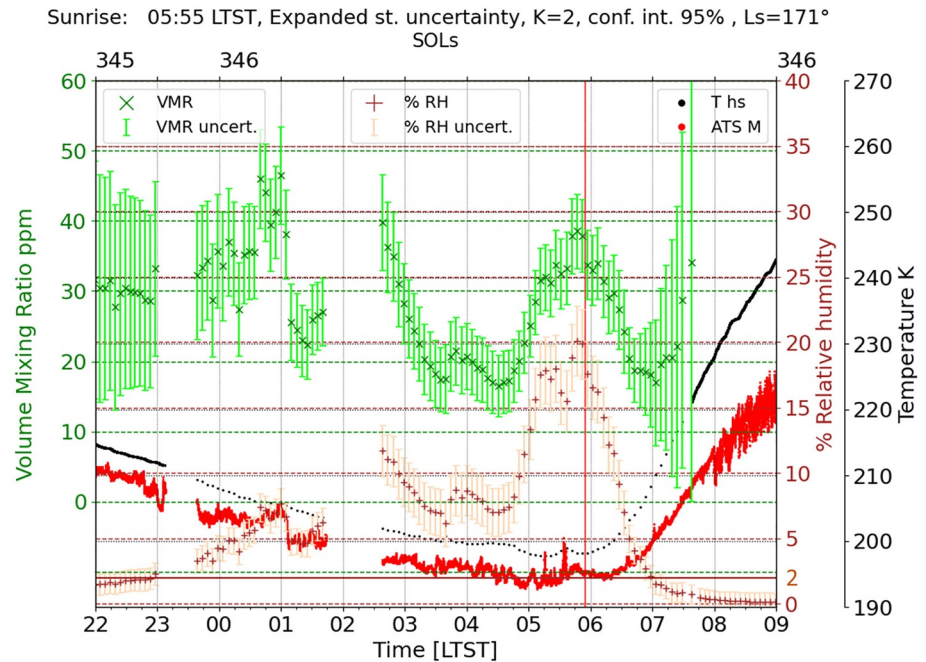


Figure 3. Volume mixing ratios (green) and relative humidity (brown) expanded standard uncertainties ($k = 2$, confidence interval 95%). The VMR is calculated here down to 0.5% Rh values for demonstrating how VMR uncertainty grows below 2% Rh, VMR becoming rather useless. T hs (black) is the humidity sensor temperature and Air Temperature Sensor (ATS) M (red) is the most single value representing less contaminated air temperature calculated from ATS sensors 1...3 (Munguira et al., 2023). Rh is referenced here to sensor T (T hs). We also see here how turbulence in ATS data bring or remove humidity (00:30–01:00 and 05:00–06:00). Gaps in the data around 23:00 and 02–03 LTST are because Mars Environmental Dynamics Analyzer has been commanded off. Solar longitude Ls = 171°.

pressure measurements, uncertainty contributed by transferring Ground Reference model results to Flight model (calibration was continued with the Ground Reference model after the delivery of the Flight and Spare models) and uncertainty contributed by water vapor enhancement factor (deviation of water vapor partial pressure from the water vapor saturation pressure approximations which are presumed to have no carrier gas mixed with the water vapor). Uncertainties were combined using quadratic law of error propagation (assuming no correlations between contributing uncertainties) (JCGM, 2008). The combined uncertainty is dominated by the uncertainty of the calibration model and nonlinearity. Water vapor enhancement factor has a negligible effect because of the very low pressure. The water vapor enhancement factor was found to be less than 0.03 (VTT-Ltd., 2022).

The lowest calibration temperature was -70 C° . Calibration and uncertainty analysis was extrapolated from -70 C° to -90 C° temperature. The best achieved combined standard uncertainty of MEDA-HS calibration for the full humidity range (0%–100% Rh) was found to be highly sensitive to the ambient temperature and the actual humidity level. With 95% confidence interval (coverage factor $k = 2$), the expanded standard uncertainty was analyzed to vary roughly between (a) 2.2%–6% Rh units in -85 C° , (b) 1.2%–4.4% Rh units in -70 C° , (c) 0.8%–3.8% Rh units in -50 C° , and (d) 0.8%–3.6% Rh units in -30 C° . These uncertainties are valid in stable conditions in pointwise measurements (stable pressure, temperature, and humidity, MEDA HS switched on for 10 s for a measurement). The accuracy of the humidity measurements is demonstrated in Figure 3. Expanded standard uncertainty (coverage factor $k = 2$, confidence interval 95%) is shown for sol 346. VMR standard uncertainty is calculated according to JCGM (2008) combining contributing uncertainties by Equation 1 and including standard uncertainty 0.11 C° for humidity sensor temperature calibration uncertainty (from calibrations) and assuming 3.5 Pa pressure standard uncertainty. Square of the VMR standard uncertainty u is given by the following Equation 1:

$$u^2 = \left| \frac{\partial \text{VMR}}{\partial \text{Rh}} \right|^2 u_{\text{Rh}}^2 + \left| \frac{\partial \text{VMR}}{\partial T} \right|^2 u_T^2 + \left| \frac{\partial \text{VMR}}{\partial P} \right|^2 u_P^2 \quad (1)$$

where u is VMR standard uncertainty and u_{Rh} , u_T , and u_p are standard uncertainties of relative humidity, temperature, and pressure.

The VMR standard uncertainty here is practically dominated by the uncertainty of the relative humidity measurement. The effect of pressure uncertainty is negligible and could be omitted. The uncertainties shown here are deviations from the calibration standard and in principle valid in laboratory conditions. The repeatability is 0.02% Rh and reproducibility 0.14% Rh. The Rh uncertainty excludes time dynamic effects and the separate measurements made at the rover level (pressure uncertainty and resistance measurement uncertainty of the humidity sensor Pt1000 platinum resistor, their contribution to total uncertainty being small). Figure 3 also demonstrates why the VMR should not be calculated below about 2% Rh values. For Figure 3, VMR values were calculated down to 0.5% Rh values. The expanded standard uncertainty ($k = 2$, 95% confidence interval) of VMR values shown start increasing below about 2% Rh values so that VMR values become unreliable. Therefore 2% Rh is used in this work as lower limit for calculating VMR or other absolute humidity values. Useful time ranges when $Rh > 2\%$ for the VMR values are visible in Figure 7. In Figure 3, we see that $Rh > 2\%$ from 23:00 LTST to about 1 hour after sunrise 07:00 LTST. Although these time limits are rather typical, using just time limits for VMR calculation alone is not recommended (Figure S2 in Supporting Information S1).

4. MEDA-HS Operations Onboard Perseverance

Health and performance of the MEDA-HS are monitored by examining the outputs of the housekeeping constant capacitors, temperature sensors, and the humidity sensor elements. The humidity sensor output during the daytime is practically the same as a dry value, as it goes below the uncertainty. This feature is used to check the stability of the sensor in flight and to monitor drift. Any significant deviation or drift of the electronics will be revealed by constant reference capacitors and multiple temperature sensors. Up-to-date, MEDA-HS electronics has been stable.

Humicap humidity sensors had some drifting upon landing on Mars, drifting was most probably caused by ingassing some volatile material during the interplanetary cruise phase or in the storage prior the launch. Drifting which was compensated by regeneration procedures at sols 63 and 73. Recovering from the regeneration itself takes few sols. Thus, the data before sol 80 are not used in this work. Regeneration has to be performed periodically to maintain accurate output and to date, the regeneration heating process has been applied four times. The first regeneration at sol 63 had a clear effect. The second regeneration was applied soon after at sol 73 showing a small effect. The sensor had obviously been contaminated after the last calibrations in 2018 either during storage or during the cruise phase or both. The third regeneration was applied on sol 180. A very small effect is barely visible after the sol 180 regeneration, well below the level of the sensor uncertainty. Regeneration effect in sol 335 had minor shift in zero %Rh level. Effects of the three first regenerations is clearly seen in the dry daytime values of the sensor (minimum %Rh per sol) shown in Figure 4.

MEDA-HS has two basic operational modes: Continuous mode (CM) and High-resolution Interval Mode (HRIM). In the continuous mode, MEDA-HS is switched on and output recorded once a second as long as the continuous mode continues. In the HRIM mode, MEDA-HS is switched on for 10 s, recorded once a second, and then switched off. The HS relative humidity output value is calculated as average of the five values starting from the third value of this 10-s time period for the both Humicap sensors separately and their average is the final value. Then this 10-s measurement is repeated after 15 or 5 min. 15 minute interval was used in the beginning of the mission, but it was later changed to 5 min beginning from the sol 146 (Ls 73.2°).

The MEDA-HS modes described above are modulated by MEDA basic measurement strategy. Because of operational limitations, MEDA is not running all the time but typically every other hour. The measured hour varies between odd and even hours of the SOL. Thus, typically MEDA-HS is powered continuously for an hour in the continuous mode or 4 or 12 times in an hour for a 10 s measurement in the HRIM mode. Occasionally MEDA has also other operational strategies and MEDA-HS is measured accordingly either in the CM or continuously running HRIM mode for period of several hours. Observation modes up to sol 410 (Ls 210°) are presented in Figure 5.

MEDA-HS heats up usually 0.6–1.2 C° during continuous mode measurements. At the start up, this causes a small deviation to the derived absolute humidity value during the first few minutes and a small increased uncertainty remains after a few minutes power on time. This nonideality is caused by small temperature gradients

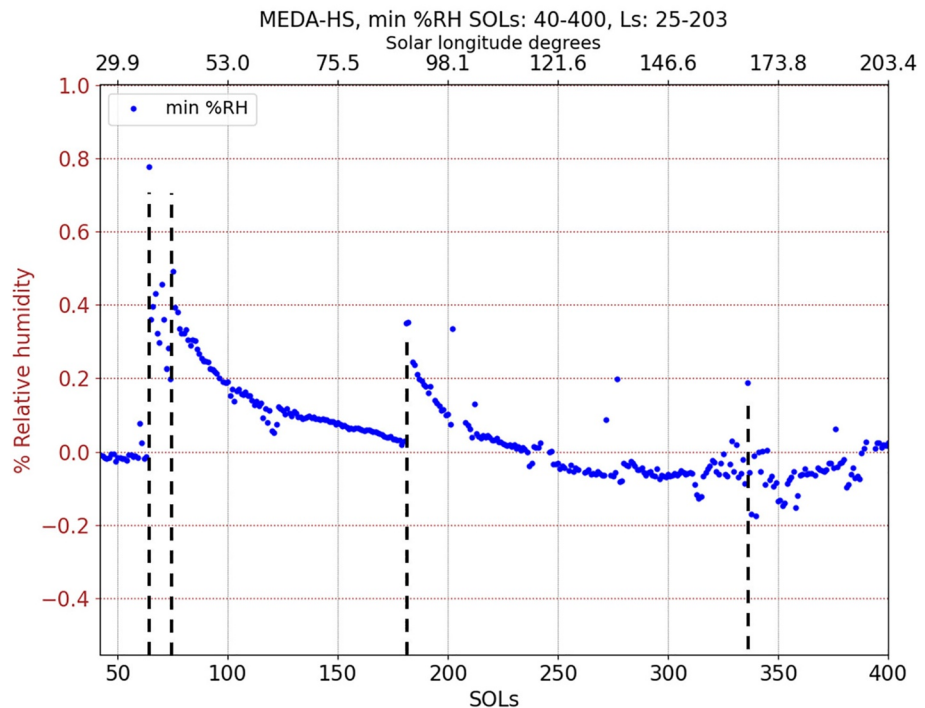


Figure 4. Minimum Rh values per sol show the effects of the regeneration in sols 63, 73, 180, and 335 (marked by vertical dashed lines). Regeneration in sol 335 is visible clearly only in the next sol. This indicates that there has been little contamination between sols 180–335. Small negative relative humidity values in the time series result from the calibration equation not being optimized for very low day time rh values and the sensor operating outside the useful range.

developing in the circuitry, for which the algorithm compensating for thermal drift cannot properly compensate. The heating in the first few seconds of the HRIM mode, after power on, is negligible, therefore the best accuracy is achieved by HRIM mode. The first few seconds of the continuous mode measurement are equivalent to the HRIM measurement. The MEDA-HS was calibrated in an HRIM-like mode. Accurate value for HRIM and CM mode calibration difference cannot be given at present. We assume the difference is on the order of 1–2 ppm in VMR based on laboratory tests and examination of the flight data. When CM mode observations were used, first eight minutes of data were not used to allow the sensor heat up and stabilize as CM starts may experience a short period extra fluctuation.

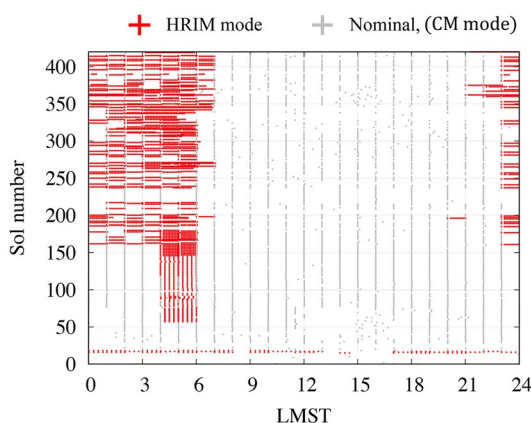


Figure 5. MEDA-HS operational modes up to sol 410 (solar longitude 210°). Red crosses show High-resolution Interval Mode observations and gray crosses show the continuous mode start times.

The MEDA-HS humidity value output has a time lag, which is on the order of minutes and depends on temperature. At the 222 K° temperature, a minute time lag was measured with the Ground Reference model (Hieta et al., 2022). At lower temperatures, the time lag increases and is estimated to be order of a few minutes in –70 C°. However, the tests never included the interface box which may have some effect on the time lag. Factors contributing to time lag are the Humicap sensor thin film membrane time constant, dust filter, and internal volume. Internal volume consists of cylindrical part housing the actual sensor compartment (the white tubular part in Figure 1, white material is the dust filter) and interface box (Figure 1). There is a narrow wire leak-through between the interface box and the sensor compartment and gas will ventilate through it. The interface box is not gas tight itself. The box was not present in the tests and therefore it is unknown how much it contributes to total time lag if anything.

5. MEDA-HS Observations and Preliminary Analyses

Volume mixing ratio (VMR) is defined and calculated by $q = e/p$, where e is water vapor pressure and p is ambient pressure. Ambient pressure is provided

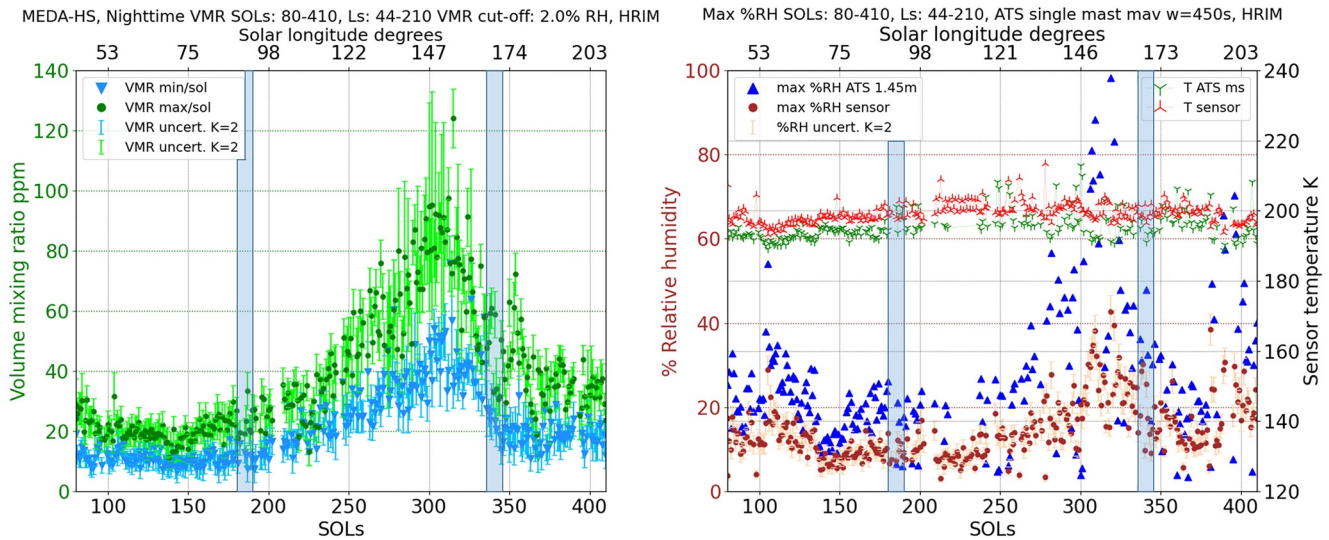


Figure 6. Nighttime volume mixing ratio max and min values per sol in the left, max %Rh values per sol in the right for sols 80–410 (Ls 44°–210°). Only High-resolution Interval Mode observations are used here. Error bars show expanded standard uncertainty ($k = 2$, confidence interval 95%). %Rh is shown both for the sensor (the output of the sensor) and the calculated %Rh for air stream using Air Temperature Sensor (ATS) air sensor values. “ATS ms” is “mast single value” representing RTG contamination free ATS sensor values in 1.45 m level from ground. “T sensor” is HS sensor temperature, the temperatures are at the time of max Rh value. Nighttime here is typically from around 23:00 LTST up to 06:00–07:00, an hour or half after sunrise, the range when sensor output Rh > 2%. Below 2% Rh, relative uncertainty grows so that VMR cannot be calculated reliably. Shaded bars show the compromised data after sensor regenerations in sols 180 and 335. Recovery time after regeneration takes few sols. It is recommended to avoid using the 10 sol data after recovery.

by the MEDA PS pressure sensor, and the value at the same time stamp as the humidity sensor value is used to calculate the VMR. If pressure data have not been available, VMR values have not been calculated. The number of these missing pressure-data gaps has been negligible. Water vapor saturation pressure is calculated using Buck-Ardenne equation (Buck, 1981), which is sufficiently accurate for our purposes (Savijärvi et al., 2015). Relative humidity (Rh) is expressed over ice, $\%Rh = e/e_s \times 100\%$, where e_s is water vapor saturation pressure over ice.

Seasonal development of nighttime humidity observations presented in Figures 6 and 7 shows diurnal values for sols 80–410 (Ls 44°–210°). Figure 6 shows nighttime volume mixing ratios (VMR) in HRIM mode per sol with expanded standard uncertainty (coverage factor $k = 2$, 95% confidence interval) and max relative humidity values per sol for both the sensor and for the air stream. VMR values are calculated for Rh values above 2% (in the sensor). In practice, Rh is below 2% from half an hour to an hour after sunrise to 21:00...24:00 LTST, depending on the sol and season (Figure 7). Max Rh in Figure 6 right is shown both for the sensor (the sensor output, relative humidity is referred to sensor temperature measured by a platinum Pt1000 thermoresistor in the sensor) and for the environment in air stream. The latter value is calculated using MEDA-ATS air-temperature sensors. The ATS single-mast value represents an estimate for air temperature free of thermal contamination from the rover, remote-sensing mast (RSM), and RTG (Radioisotope Thermal Generator) power source. Depending of the wind speed and direction ATS sensors 1, 2, and 3 located around the RSM at the same height 1.45 m feel different thermal contamination from rover’s RTG. ATS Mast single value is calculated using the values of the ATS 1, 2, and 3. Practical nighttime approximation for the ATS Mast single value is the lowest value of the three ATS sensors which works for humidity sensor accuracy and time resolution. ATS 1...3 sensor values and ATS single mast value have been provided by MEDA-ATS team (Munguira et al., 2023). ATS sensors react fast for turbulence. Moving average over 450 s was applied to ATS single mast values before calculating relative humidity. Rh error bars are shown only for the sensor humidity values, it was not possible to calculate uncertainties for air stream humidity as ATS single value uncertainty is not available. We assume here that water vapor pressure in the sensor (inside the dust filter) is the same as in the air at about the same level from ground and calculate Rh in air directly $Rh_{air} = e/e_s(T_{ATS}) \times 100\%$, where $e_s(T_{ATS})$ is water vapor saturation pressure over ice in air temperature $T_{ATS} =$ ATS single value. Figures S1 and S2 in Supporting Information S1 show more details of seasonal VMR and diurnal cycles.

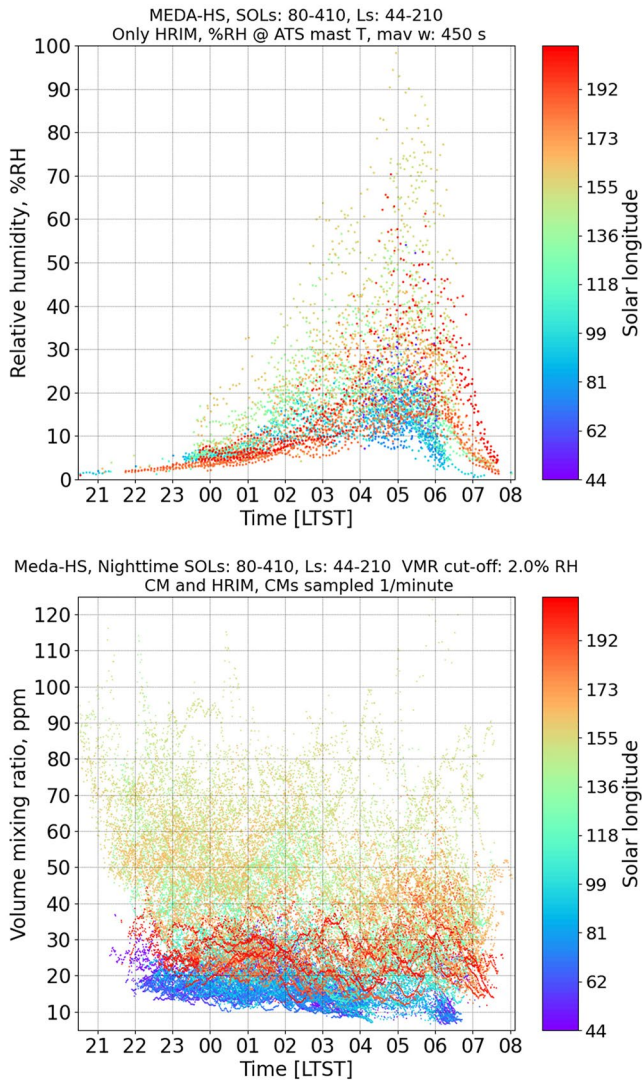


Figure 7. Upper: Nighttime relative humidity calculated for air stream (referenced to Air Temperature Sensor mast single value temperature) and Lower: Nighttime volume mixing ratios, for sols 80–410, Ls 44°–210°. Peak 100% Rh value was achieved at Sol 319, Ls 157°.

Rh values for air stream are significantly higher than the Rh sensor values. This is because the HS sensor temperature is few degrees higher than the ATS single mast value representing ATS RSM temperature data with minimal thermal contamination from RTG. The MEDA-HS sensor receives conducted heat from the rover and RSM through mounting and electric wires. Also probably some radiated heat from the rover body and mast is received too. MEDA-HS is located above the ATS 2 sensor. ATS sensors 1...3 are 1.45 m from ground and MEDA-HS 1.50 m.

Seasonal changes from Ls = 44° to Ls = 210° are seen in both the relative humidity and volume mixing ratio time series. This is caused by the pulse of water vapor generated by evaporation from the northern pole due to the heating by increased solar irradiation during northern spring and summer. Airborne water vapor is deposited on the Northern polar cap during wintertime and released back to the atmosphere with seasonally increasing solar irradiation. This water pulse is detected by the MEDA-HS humidity observations a few sols earlier than by similar instrument REMS-H onboard MSL Curiosity rover due to the fact that Curiosity is located at a lower latitude (S 4.6°) than Perseverance (N 18.4°). MEDA-HS observed humidity peak is at around Ls = 150°. The Curiosity REMS-H instrument has seen this peak close to Ls = 160° (this current Mars year MY = 36) (Figure 8). This peak humidity period was also covered by an increase of dust activity and the later dust storm from Ls = 153° to Ls = 156° (Lemmon et al., 2022).

Diurnal humidity cycles are shown in Figure 7. Relative humidity peaks near the coldest time of the night just before sunrise. During the daytime, the %Rh is below uncertainty of the sensor. The VMR slowly decreases during nighttime, which is most likely caused by adsorption in the regolith (Savijärvi et al., 2019). The VMR nighttime trends for dry season and wet season are shown right in Figure 9. The data also exhibit short-timescale (subhour) humidity fluctuations (Figure 9 left). They are too fast due to adsorption/desorption by regolith but are rather caused by humidity advected through turbulence from above. The nighttime atmospheric humidity increases vertically and especially above the boundary layer, there is reservoir of humid air (Savijärvi et al., 2019) that can serve as a source of humidity for turbulence. The nighttime humidity fluctuations are due to the wind capable of creating turbulence sufficient to bring humidity toward lower altitudes. The great wind variability observed by Mars 2020 at night/early morning was consistent with an increase in mechanical turbulence caused by downslope convergent flows on the crater floor (Viúdez-Moreiras, de la Torre, et al., 2022;

Viúdez-Moreiras, Lemmon, et al., 2022). Figure 10 shows continuous-mode observations of the nights of sols 330/331 and 399/400. The changes of the humidity VMR levels at 01:50–02:20 LTST/sol 331 and 03:00–03:30 LTST/sol 400 are related to air temperature changes, suggesting change in the wind direction (more thermal contamination from RTG is observed by ATS sensors during those time periods). This turbulence in wind may also break the nighttime boundary layer and bring humid air from there (Pla-García et al., 2020). Figure 11 shows in detail temperature observations for the nights 330/331 and 399/400 including 40-m temperature provided by MEDA-TIRS sensor (Sebastián et al., 2021). Temperature jump is visible in all the levels during the VMR level changes. This may result from nocturnal downslope flow or from the peak of a nocturnal low level jet (Chatain et al., 2021; Savijärvi and Siili, 1993).

Fluctuations are also shown in Figure 12 with HRIM observations. While the temperatures are slowly declining and the Rh% is slowly increasing over the nighttime, no average decline of absolute humidity level is visible in the VMR, actually a small increase instead. Fluctuations seem to be related in turbulence shown by air temperature data here too.

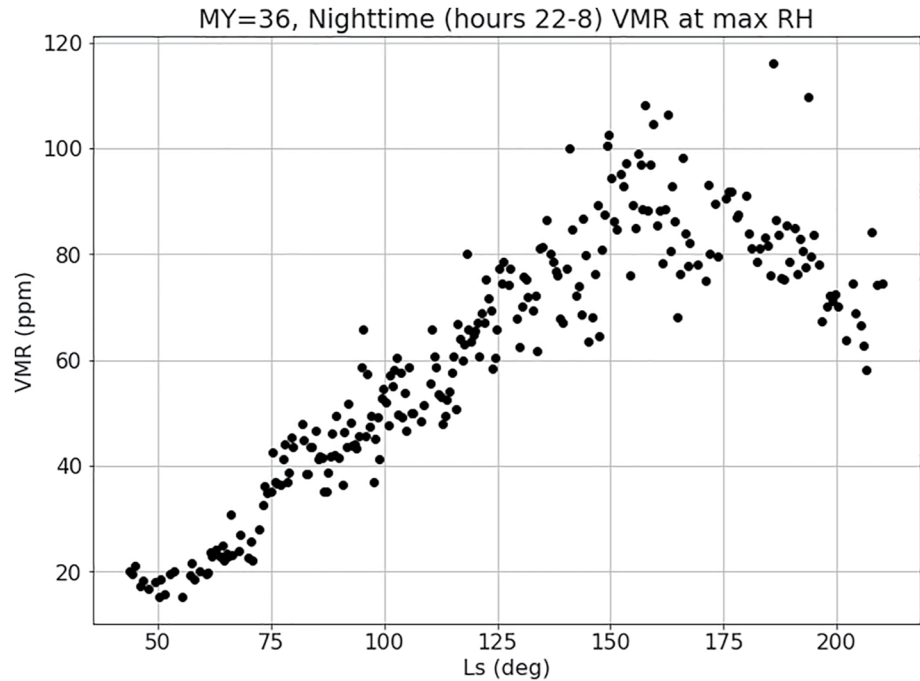


Figure 8. Mars Science Laboratory Curiosity relative humidity sensor REMS-H VMR time series for Ls 44°–210°. Seasonal humidity peak is around Ls 160°.

Both Figure 10 (left plot) and Figure 12 show an unexpected fall of VMR after sunrise when it is expected to be rising. Owing to heating of the surface and likely desorption of vapor, the VMR is expected to rise as the day warms, but because the relative humidity drops below sensor's sensitivity, this is not observed. This decrease in VMR after dawn is seen in many sols (e.g., in sols 319, 330, 334, 341, 342, and 362). An explanation for this “bending” VMR in dawn could be dry air advecting over the terminator from the night side. More details shown in Figures S3 and S4 in Supporting Information S1.

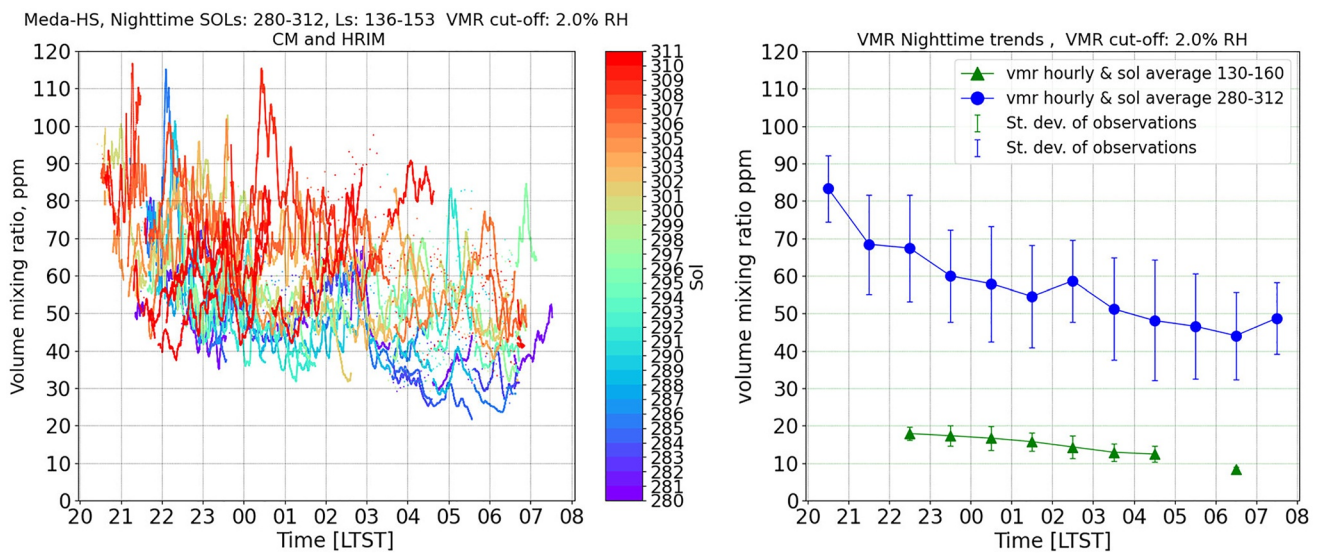


Figure 9. In the left: Short timescale humidity fluctuations in detail in the sols 280–312, Ls 136°–153°. In the right: VMR hourly averaged values over period of sols show nighttime trends for the dry season (sols 130–160, Ls 66°–80°, green) and the wet season (sols 280–312, blue). Error bars show standard deviation of the observed values in the hour slice. Sunrises are in the sol 145, Ls 73° at 05:25 LTST, and in the sol 296, Ls 144° 05:39 LTST. Continuous mode observations were used to calculate hourly averages. Gap in the sols 130–160 data in the 05–06 LTST hr slice is because of missing CM mode observations.

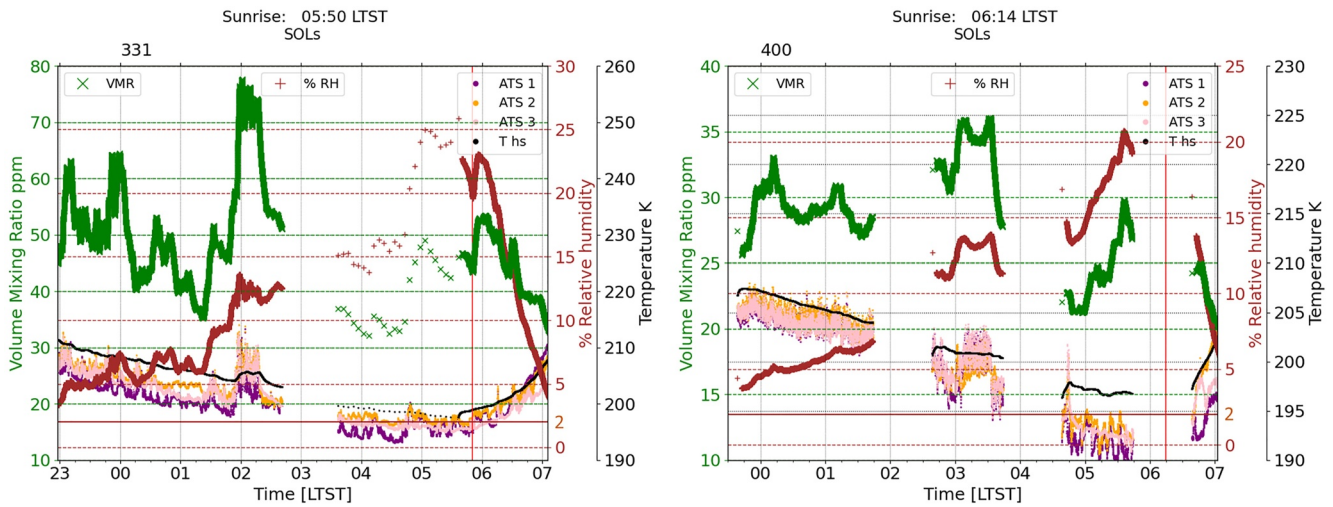


Figure 10. Typical short-term humidity fluctuations shown in sol 331 (Ls 163°) and sol 400 (Ls 203°). Red vertical line shows sunrise time. Rh shown here(%RH, brown) is at the HS sensor referred to HS temperature sensor (T hs, black), all three of the remote-sensing mast Air Temperature Sensor (ATS) sensors 1–3 are shown. In the left plot, 01:50 turbulence seen in the ATS data indicates a wind change, which brings more humid air. HS sensor T sensor warms up, too, but humidity pulse is strong enough to also keep Rh up. On the right, there is similar event from 03:00–03:45.

Uncertainties of the MEDA-HS and -TIRS sensors were used to evaluate the probability for surface frosting conditions. Here, we assume a well-mixed surface layer from the ground to the 1.5-m sensor height so that the absolute humidity is vertically constant. Surface temperature T_g observed by MEDA-TIRS ground temperature sensor has fallen below the calculated frost point T_f on several nights (Figure 13).

Most likely frost events have been in sols 381, 382 (Ls 192°), 398 (Ls 202°), and 402 (Ls 205°) where condition requirement $T_g < T_f$ has been exceeded over confidence interval 99.7%, coverage factor of standard uncertainty $k = 3$ filling $T_g + ku(T_g) < T_f - ku(T_f)$, where $u(T_g)$ = standard uncertainty of ground temperature T_g and $u(T_f)$ = standard uncertainty of frost point T_f (Martínez et al., 2016). Likelihoods for frosting conditions are presented in Figure 13 rightside plot.

Figure 14 shows nighttime evolution of T_f and T_g for sols where $k > 2$ for possible frost events. Events have been close to coldest time of the night. Figure 15 shows the MEDA-TIRS field of view of the terrain for sols where

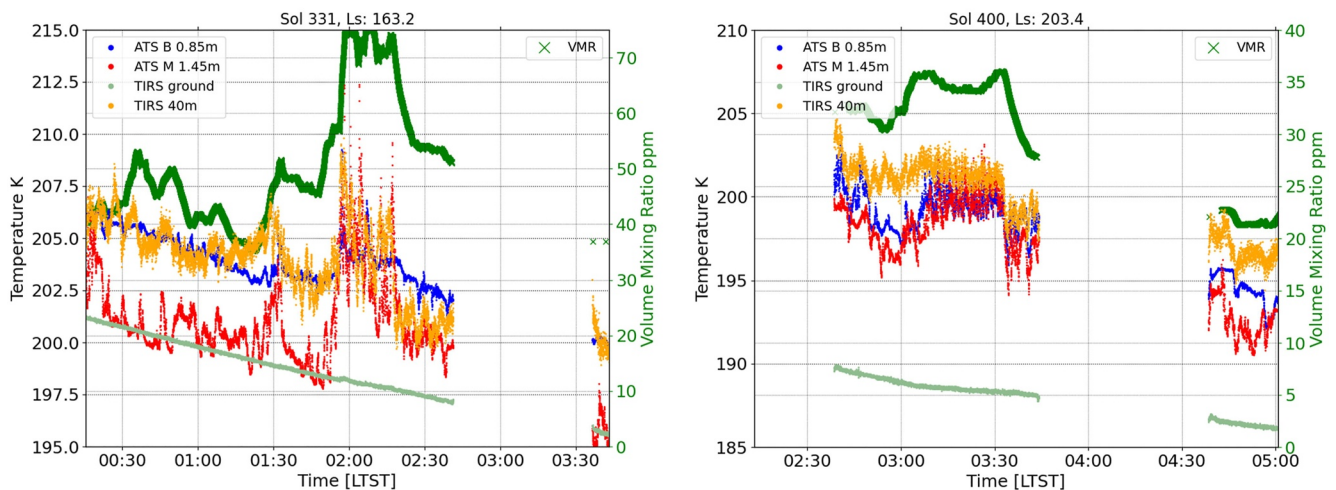


Figure 11. Turbulence in temperature data in more detail for early morning night events sols 331 and 400. In the left plot, at LTST 01:50...02:20 and in the right plot LTST 03:00...03:45, also the 40 m level temperature (TIRS 40 m provided by MEDA-TIRS sensor) reacts as well as other levels. Air Temperature Sensor (ATS) M 1.45 m is ATS single value at mast sensor level and ATS B 0.85 m is single value representing ATS sensors 4 and 5 located at the front of rover body. TIRS ground is surface T provided by TIRS.

Night Sols: 407-408, P. ave: 714.0Pa, Ls: 207.8 vmr cut-off:2.0%Rh Sunrise: 06:17 LTST
SOLS

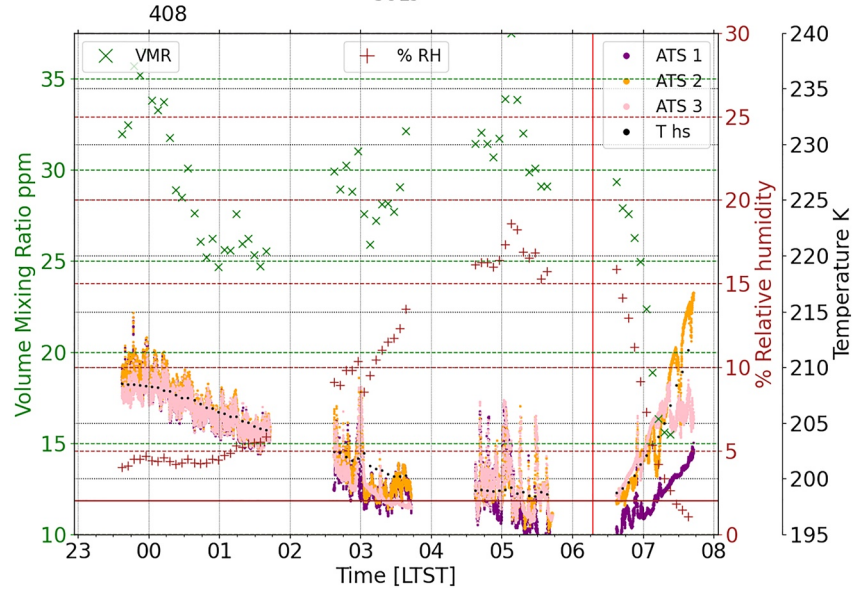


Figure 12. Typical short-term humidity fluctuations shown in sol 408 (Ls 208°) using High-resolution Interval Mode data. Red vertical line shows sunrise time. Rh and Air Temperature Sensor like in Figure 10.

$k > 2$ has been reached. In each case, the terrain was composed of fine-grained material with low thermal inertia (Martínez et al., 2023), which results in relatively colder nighttime temperatures. Thus the most possible frost events have been caused by ground temperature being unusually low not humidity being high.

6. Single Column Model Comparison With Measurements

Here the diurnal cycles of MEDA HS observations are shown for sols 138–148 (Ls 70°–74°, low VMR) and sols 290–300 (Ls 141°–146°, high VMR) together with results from the UH/FMI adsorptive single-column model (SCM, Savijärvi and Harri, 2021; Savijärvi, Martinez, Harri, and Paton, 2020; Savijärvi et al., 2016, 2022).

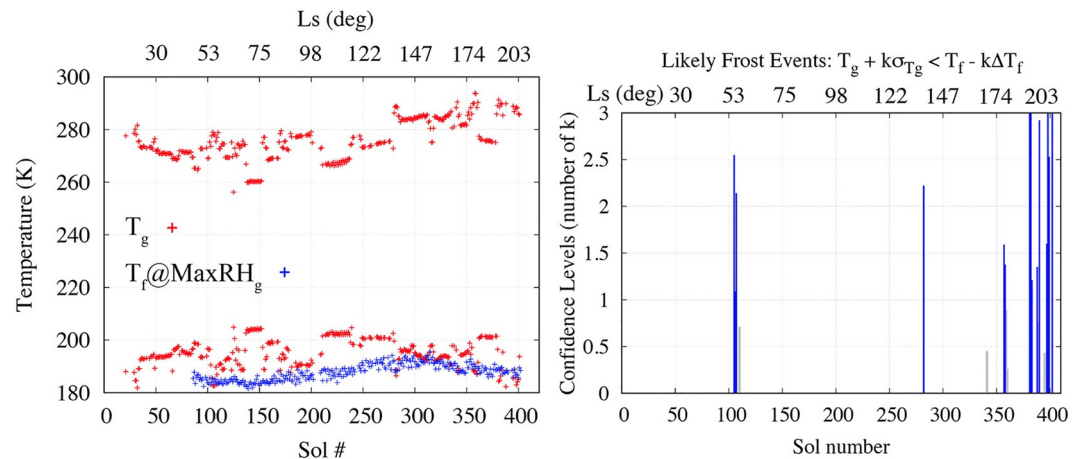


Figure 13. Daily maximum and minimum ground temperature (red) and frost point temperature when the Rh at the ground is maximum (blue) as a function of sol number and Ls during the first 410 sols of the M2020 mission. Potential frost events are identified when $T_g < T_f$. (right) Likelihood of potential frost events represented by the number (coverage factor k) of standard uncertainty in T_g and uncertainty in T_f for which the relation $T_g + ku(T_g) < T_f - ku(T_f)$ is met.

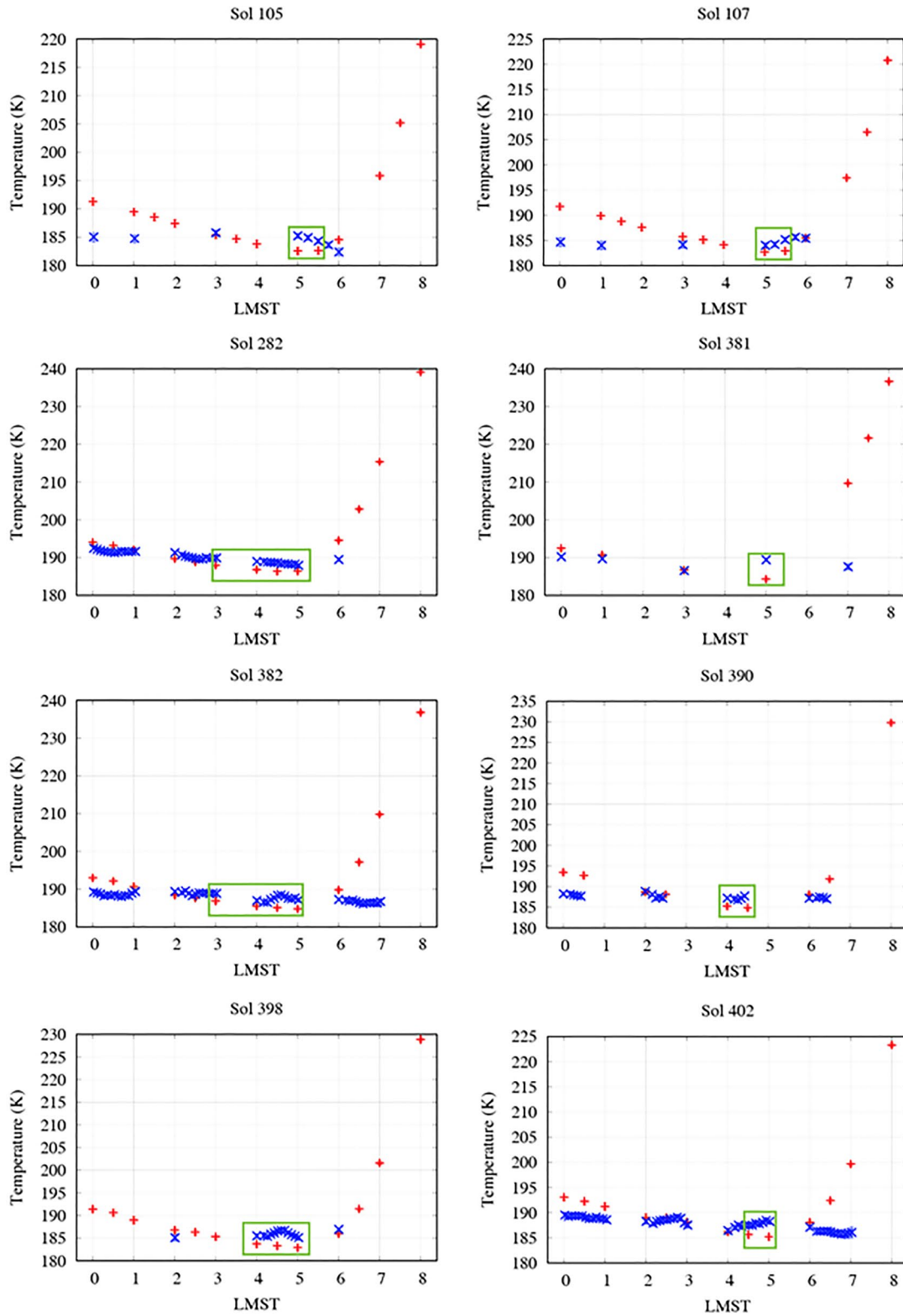


Figure 14. Nighttime evolution of ground temperature (red) and frost point temperature (blue) in sols when the likelihood of frost events is high ($k > 1$). In these sols, $T_g < T_f$ between 03:00 and 06:00 LMST, corresponding to the coldest time of the sol.

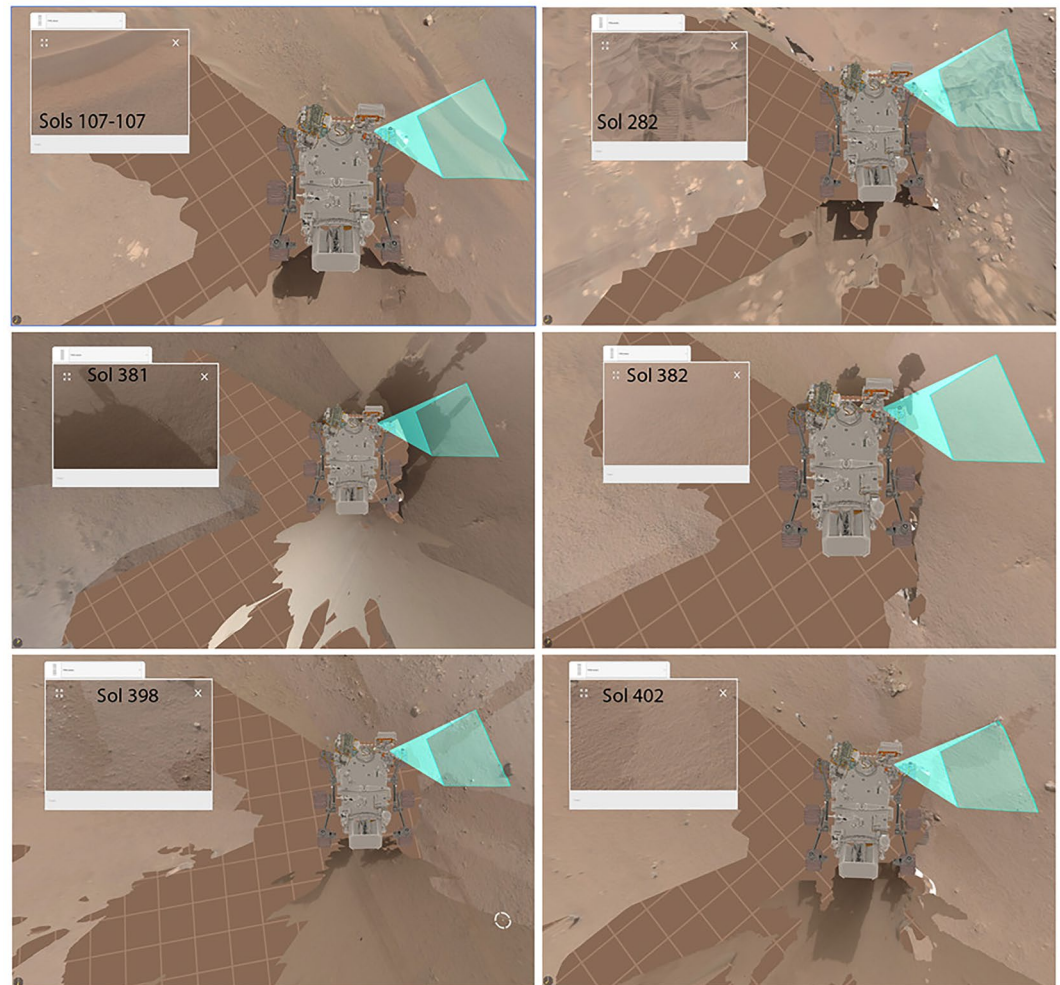


Figure 15. Mars Environmental Dynamics Analyzer/TIRS field of view of the terrain in sols when the likelihood of frost events is high ($k > 1$ in Figure 13). In each case, the terrain was composed of fine-grained material with low thermal inertia (Martínez et al., 2023), which results in relatively colder nighttime temperatures.

During Ls 70°–74°, in the aphelion period of very low moisture, the rover was stationary with observed surface pressure of 750 hPa, dust opacity 0.4, and surface albedo 14%. Thermal Emission Spectrometer (TES, onboard Mars Global Surveyor) Ls 60°–80° observations suggest precipitable water column (PWC) of about 5–6 μm over Jezero (Steele et al., 2017). For well-mixed moisture the volume mixing ratio (VMR) is then about 70 ppm. These values initialized our SCM simulations for Ls 72° (sol 143). MEDA-TIRS ground temperature observations of this period suggest ground thermal inertia I of about 600 SI units, while Pla-García et al. (2020) used 260. Hence I -values of 300, 400, and 600 were tried. Figure 16 shows the resulting model-VMR curves. The dashed curve is a simulation without adsorption, where only diffusion to/from porous ground acts to slightly change the near-surface air-VMR from its daytime well-mixed value of 70 ppm. Porosity (air fraction of regolith) here is 25% resulting in model-PWC staying around 5.3 μm from sol to sol.

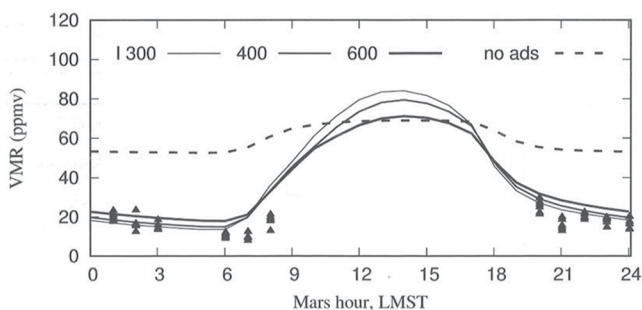


Figure 16. Tuning single-column model parameters with different thermal inertias 300, 400, and 600 for the sol 143. Dashed line show no adsorption case. Triangle dots are VMR hourly observations by MEDA-HS for sols 138–148.

Figure 17 left displays for sols 138–148 the MEDA-HS humidity values at 1.5 m height and ATS mast single values for air temperature at 1.45 m height together with the respective SCM curves, and also the SCM-predicted surface temperature and VMR. Rover's energy source RTG dissipates heat and this may occasionally disturb the ATS sensors. We see this effect from

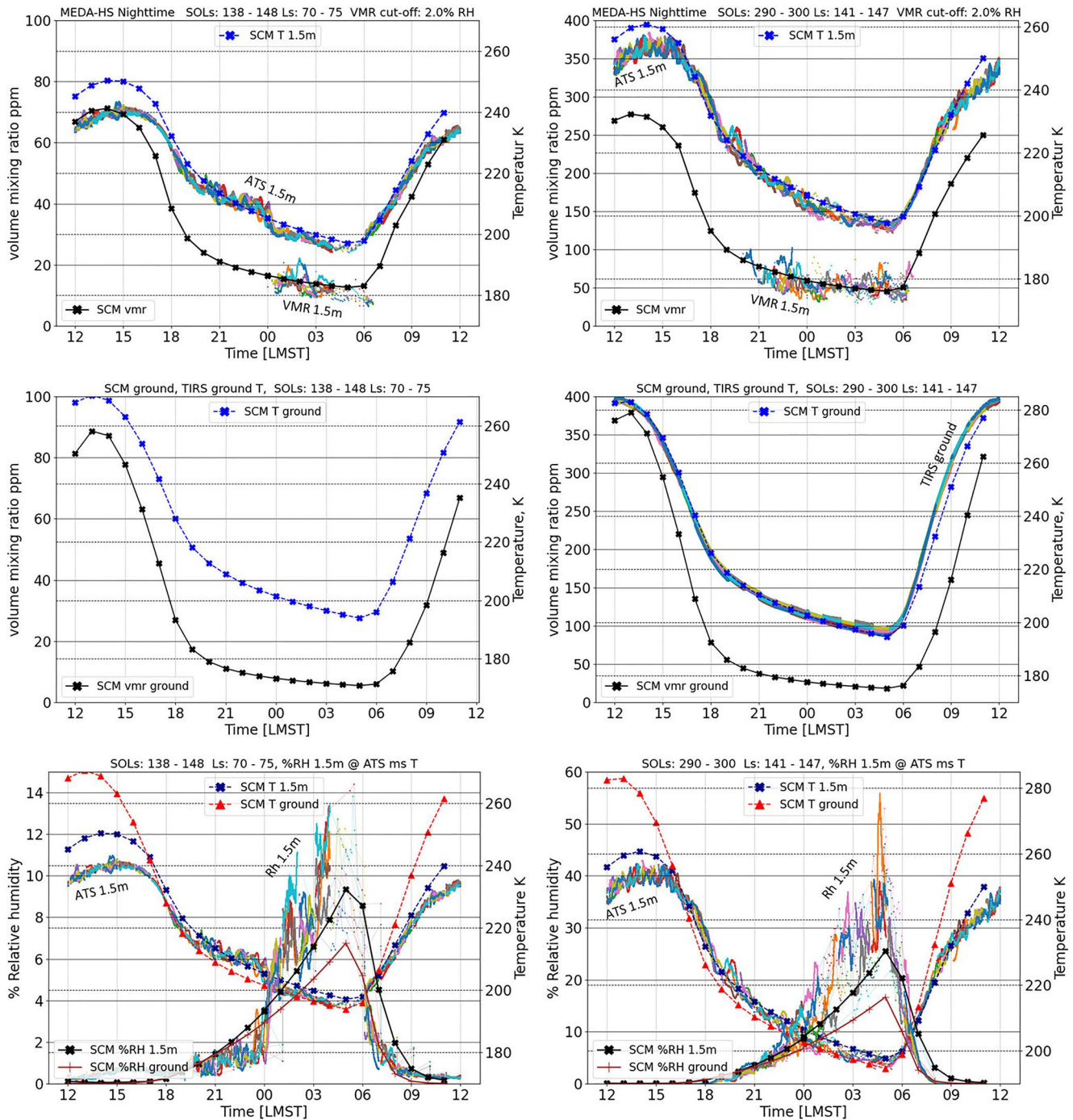


Figure 17. Single-column model (SCM) results compared to observations. Left: Sol 143 model compared to sols 138–148. Right: Sol 295 model compared to sols 290–300. Upper: HS and Air Temperature Sensor (ATS) observations at 1.5 m level compared to SCM at 1.5 m. Middle: SCM VMR and ground T compared to Mars Environmental Dynamics Analyzer TIRS ground temperature observations. In the sol 138–148 range TIRS ground sensor was pointing to a spot which was not representative for the area and produced too high readings, so they are not shown. Lower: SCM Rh and SCM T at 1.5 m and ground level shown together with 1.5 m HS and ATS observations. 600 second moving average was applied to ATS values.

22:00–00:00 LMST, the ATS mast single value dropping suddenly after midnight. Rover's stern with RTG was pointing at the west and wind has been from west so that the heated plume hit directly RSM with ATS sensors. At midnight, small changes in wind direction and speed removed this thermal contamination from the ATS sensors and their values dropped. This effect is also visible in relative humidity values, which are referred here

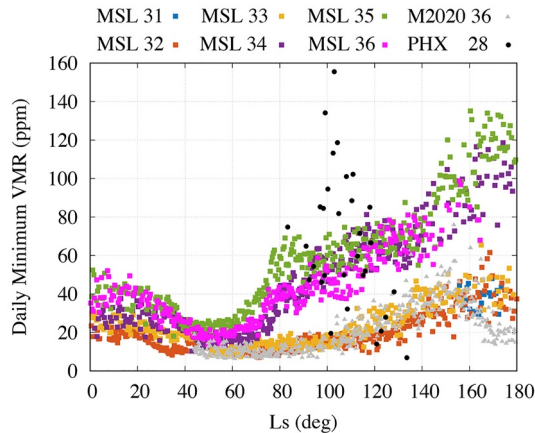


Figure 18. Comparison of Mars Science Laboratory, Phoenix (PHX), and M2020 Perseverance in situ humidity observations. Number after mission refers to Martian Year.

as the ATS mast single values. The best model fit to observed Rh is obtained with $I = 350$ SI units. The minimum VMR here around sunrise is only about 15 ppm, which fits to the MEDA-HS observations. Maximum daytime model-VMR is slightly above 70 ppm, which fits to the TES PWC of 5–6 μm . Thus with adsorption the model results become quite close to the MEDA-derived very low nighttime VMR during this period.

For the humid period at $L_s 141^\circ\text{--}146^\circ$ (sol 295 nominal), the CRISM mean value of 14.4 μm PWC of the season over Jezero (M. D. Smith et al., 2018) was used for initialization. Observed surface pressure here was 626 Pa, dust opacity 0.5, and albedo 12%. With thermal inertia of 320 SI units and porosity of 25%, the SCM results fit here well to the observed air and ground temperatures and to the high air moistures (Figure 17, right), conserving the well-mixed daytime VMR at 270 ppm and PWC at 14.4 μm from sol to sol with VMR dropping to 50 ppm at each sunrise. Model output at 1.5 m and ground level can then be used for estimating ground level relative humidities and VMR from the 1.5 m observations, assuming the same proportional relation as the model, respectively, had.

The model results (Figures 16 and 17) hence indicate that adsorption/desorption is here the main reason for the diurnal water exchange between atmosphere and regolith, suggesting enthalpy of about 22 kJ/mol for the process (independently of the mineralogy, Savijärvi and Harri (2021)) with porosity of regolith being about 25% at the two sites.

7. Conclusions and Discussion

The MEDA-HS relative humidity sensor on board the M2020 Perseverance rover has produced in situ relative humidity observations useful from the sol 80 ($L_s 44^\circ$) onward. Two observational modes have been used, point-wise measurements, High resolution Interval mode (HRIM) has been taken once per 15 min or 5 min while continuous mode observations (CM) provide readings once per second. Time lag of the sensor is estimated to be order of few minutes in nighttime temperatures. HRIM mode offers better accuracy than CM mode. Exact difference between the modes will be studied further later. Sensor output is used to calculate derived volume mixing ratio VMR when relative humidity of the sensor is above 2%, when below, VMR values become too inaccurate. VMR values are available thus for nighttime only, from around 22:00 LTST to few tens of minutes after sunrise. Peak relative humidity is reached around the coldest time of the night, which is usually just before sunrise. At daytime relative humidity is below resolution of the sensor. MEDA-HS temperature is few degrees higher than air temperature at the same level from the ground, thus if relative humidity value is used, it should be transferred to air temperature using MEDA-ATS air temperature sensors.

Initial results from the sols 80–410 ($L_s 44^\circ\text{--}210^\circ$) show how seasonal water vapor pulse is released from northern ice cap reaching peak at $L_s 150^\circ$. The highest recorded nighttime VMR value was 120 ppm at sol 315 ($L_s 154^\circ$) and peak Rh value was 100% (referenced to ATS air temperature at 1.45 m level) at sol 319 ($L_s 157^\circ$). These values were single peaks at isolated sols while the seasonal peak appears to have been few sols earlier. Pointing exact sol and peak values depends on whether CM mode measurements are included. It is not likely that this difference depends on possible calibration level difference between HRIM and CM mode but rather availability of measurements and operational cadences which alternate from time to time. There have been more CM mode observations at early night hours.

Nighttime observations show large short time scale (sub hour) humidity fluctuations. VMR levels show slowly declining level at night average over several sols, but there are large variations. On some single sols, VMR level may be even at higher level just before sunrise than early night hours. Fluctuations are most likely caused by humid air entering from above the rover or even from above boundary layer because of turbulences. The level changes often coincide with strong turbulence seen in ATS air temperature data.

Frost point may have been reached on ground on few sols between $L_s 192^\circ$ and 205° , assuming constant volume mixing ratio profile from the sensor level to ground.

Adsorptive SCM was tested and compared with the MEDA-HS observations for two cases, sol 143 (dry season) and sol 295 (humid season). Good model fits to nighttime T, Rh, and the derived VMR observations were

obtained assuming adsorption. The observation-based VMR indicates strong nighttime adsorption of water vapor into soil. The SCM model can be used for estimating surface humidity by transferring observations at 1.5 m to ground level. The model is also able to include underground humidity as water vapor in airspaces of the porous ground.

The MSL, Phoenix (PHX), and M2020 Perseverance humidity observations are compared in Figure 18. The daily VMR minimum typically occurs between 03:00 and 06:00 LMST at MSL and M2020 and between 02:00 and 04:00 LMST at PHX. Interestingly, VMR values in Martian Year (MY) 36 at MSL (magenta) are higher than at M2020 (gray), despite column abundances of water vapor being larger at M2020 than at MSL. At PHX (black), VMR values peaked around Ls 105° when column abundances were largest due to the sublimation of the northern polar cap. Then, VMR values rapidly decreased when temperatures dropped and water vapor was deposited on the surface (Fischer et al., 2019; Martínez et al., 2017).

Liquid water is a requirement for life as we know it on Earth, which is why its abundance and distribution on Mars are key metrics with regard to characterizing the habitability potential of Mars, past and present. Measurements that facilitate an understanding of the present hydrologic cycle at the surface of Mars in Jezero Crater likely provide a glimpse of the lower limit of water abundance, near the surface and potentially available to the shallow subsurface (to perhaps a few mm). If water is transferred to the surface as our nocturnal volume mixing ratios suggest, the adsorbed water could be available to hydrate a shallow subsurface cryptoendolithic habitat, if one exists. Such a habitat, a community of organisms living in the pore spaces of rock, can be observed in sandstones in the McMurdo Dry Valleys of Antarctica on Earth (Imre Friedmann, 1982). If the current water cycle is a historic lower bound on the amount of water transferable to the surface material, possible past microbial life that required more water may have left chemical biosignatures in the coarser grained rocks. Such putative life may have adapted to an environment that could provide some protection from desiccation and radiation as the surface of Mars grew more arid.

On Earth, rock dwelling consortia of organisms may contain different species than soil dwelling organisms proximal to the rock, for example, Young et al. (2008). As Choe et al. (2021) and others have observed, climate is a dominant factor in the diversity of both types of communities, and in particular, relative humidity and precipitation (e.g., Böhm et al., 2020; CáCeres et al., 2007). Desiccation resistant organisms have been well studied in both hot and cold deserts on Earth in search of suitable Mars analog environments from which to model microbial survival strategies for an environment as water poor as the present Martian surface. What we know from the most arid environment on Earth, the Atacama Desert of Chile, is that even in this most arid of environments, various microorganisms have adapted to these conditions. Navarro-González et al. (2003) have identified the Atacama Desert's Yungay region as a good Martian analog because it is near the dry limit of life. Azua-Bustos et al. (2015) described another site, Maria Elena South, that is even drier than Yungay. Interestingly the mean Rh of the soil at a depth of 1 m is 14%, even when atmospheric Rh drops to 0 during diurnal cycles. This is associated with no decrease in microbial diversity at this depth relative to the diversity at the surface, which enjoys a mean value of 27.5%. Thus the driest environment on Earth supports microbial communities with a mean soil Rh of 14%. Our measurements would suggest a mechanism for attaining sufficient hydration to speculate that a refugium environment could have been supported even with present levels of water exchange with the Martian surface and be consistent with the most hyper arid conditions we can identify on Earth.

Data Availability Statement

Observation data used for this work are available in Planetary Data System Atmospheres node (Rodríguez-Manfredi & de la Torre Juarez, 2021). Derived data and SCM model data are available in the Finnish Meteorological Institute repository archive (Polkko, 2022). Mars Science Laboratory REMS-H instrument data used for comparison are available in Planetary Data System Atmospheres node (Gomez-Elvira, 2013).

References

- Aoki, S., Vandaele, A. C., Daerden, F., Villanueva, G. L., Liuzzi, G., Thomas, I. R., et al. (2019). Water vapor vertical profiles on Mars in dust storms observed by TGO/NOMAD. *Journal of Geophysical Research: Planets*, 124(12), 3482–3497. <https://doi.org/10.1029/2019JE006109>
- Azua-Bustos, A., Caro-Lara, L., & Vicuña, R. (2015). Discovery and microbial content of the driest site of the hyperarid Atacama Desert, Chile. *Environmental Microbiology Reports*, 7(3), 388–394. <https://doi.org/10.1111/1758-2229.12261>

Acknowledgments

Authors thank M2020 Perseverance team engineers and scientists for their commitment and work for the mission. Authors are thankful for M2020 science team and atmospheric working group for the helpful discussions and support for the instrument and running the MEDA experiment. Authors thank MEDA team for all the work for making various components of MEDA working together and for receiving and archiving the data. Jouni Polkko, Ari-Matti Harri, Maria Hieta, and Iina Jaakonaho are thankful for the Finnish Academy Grant 310509. Part of the research was carried out at the Jet Propulsion Laboratory, California Institute of Technology, under a contract with the National Aeronautics and Space Administration (80NM0018D0004). A. Vicente-Retortillo is supported by the Spanish State Research Agency (AEI) Project No. MDM-2017-0737 Unidad de Excelencia “María de Maeztu”- Centro de Astrobiología (INTA-CSIC).

- Banfield, D., Stern, J., Davila, A., Johnson, S. S., Brain, D., Wordsworth, R., et al. (Eds.) (2020). Mepag (2020), Mars scientific goals, objectives, investigations, and priorities: 2020 (white paper), (White paper posted March, 2020 by the Mars exploration program analysis group (MEPAG)). Retrieved from <https://mepag.jpl.nasa.gov/reports.cfm>
- Böhm, C., Reyers, M., Schween, J. H., & Crewell, S. (2020). Water vapor variability in the Atacama Desert during the 20th century. *Global and Planetary Change*, *190*, 103192. <https://doi.org/10.1016/j.gloplacha.2020.103192>
- Buck, A. L. (1981). New equations for computing vapor pressure and enhancement factor. *Journal of Applied Meteorology*, *20*(12), 1527–1532. [https://doi.org/10.1175/1520-0450\(1981\)020<1527:NEFCVP>2.0.CO;2](https://doi.org/10.1175/1520-0450(1981)020<1527:NEFCVP>2.0.CO;2)
- Cáceres, L., Gómez-Silva, B., Garró, X., RodríGuez, V., Monardes, V., & McKay, C. P. (2007). Relative humidity patterns and fog water precipitation in the Atacama Desert and biological implications. *Journal of Geophysical Research*, *112*(G4), G04S14. <https://doi.org/10.1029/2006JG000344>
- Chatain, A., Spiga, A., Banfield, D., Forget, F., & Murdoch, N. (2021). Seasonal variability of the daytime and nighttime atmospheric turbulence experienced by InSight on Mars. *Geophysical Research Letters*, *48*(22), e95453. <https://doi.org/10.1029/2021GL095453>
- Choe, Y.-H., Kim, M., & Lee, Y. K. (2021). Distinct microbial communities in adjacent rock and soil substrates on a high arctic polar desert. *Frontiers in Microbiology*, *11*. <https://doi.org/10.3389/fmicb.2020.607396>
- Christensen, P. R., Anderson, D. L., Chase, S. C., Clark, R. N., Kieffer, H. H., Malin, M. C., et al. (1992). Thermal emission spectrometer experiment: Mars observer mission. *Journal of Geophysical Research*, *97*(E5), 7719–7734. <https://doi.org/10.1029/92JE00453>
- Clancy, R. T., Grossman, A. W., & Muhleman, D. O. (1992). Mapping Mars water vapor with the very large array. *Icarus*, *100*(1), 48–59. [https://doi.org/10.1016/0019-1035\(92\)90017-2](https://doi.org/10.1016/0019-1035(92)90017-2)
- Clancy, R. T., Grossman, A. W., Wolff, M. J., James, P. B., Rudy, D. J., Billawala, Y. N., et al. (1996). Water vapor saturation at low altitudes around Mars aphelion: A key to Mars climate? *Icarus*, *122*(1), 36–62. <https://doi.org/10.1006/icar.1996.0108>
- Conrath, B., Curran, R., Hanel, R., Kunde, V., Maguire, W., Pearl, J., et al. (1973). Atmospheric and surface properties of Mars obtained by infrared spectroscopy on mariner 9. *Journal of Geophysical Research*, *78*(20), 4267–4278. <https://doi.org/10.1029/JB078i020p04267>
- Encrenaz, T., Lellouch, E., Cernicharo, J., Paubert, G., & Gulkis, S. (1995). A tentative detection of the 183-GHz water vapor line in the Martian atmosphere: Constraints upon the H₂O abundance and vertical distribution. *Icarus*, *113*(1), 110–118. <https://doi.org/10.1006/icar.1995.1009>
- Encrenaz, T., Lellouch, E., Paubert, G., & Gulkis, S. (2001). The water vapor vertical distribution on mars from millimeter transitions of HDO and H₂¹⁸O. *Planetary and Space Science*, *49*(7), 731–741. [https://doi.org/10.1016/S0032-0633\(01\)00009-5](https://doi.org/10.1016/S0032-0633(01)00009-5)
- Encrenaz, T., Melchiorri, R., Fouchet, T., Drossart, P., Lellouch, E., Gondet, B., et al. (2005). A mapping of Martian water sublimation during early northern summer using OMEGA/Mars Express. *Astronomy and Astrophysics*, *441*(3), L9–L12. <https://doi.org/10.1051/0004-6361:200500171>
- Farmer, C. B., Davies, D. W., Holland, A. L., Laporte, D. D., & Doms, P. E. (1977). Mars: Water vapor observations from the Viking orbiters. *Journal of Geophysical Research*, *82*(B28), 4225–4248. <https://doi.org/10.1029/JS082i028p04225>
- Fedorova, A., Korablev, O., Bertaux, J.-L., Rodin, A., Kiselev, A., & Perrier, S. (2006). Mars water vapor abundance from SPICAM IR spectrometer: Seasonal and geographic distributions. *Journal of Geophysical Research: Planets*, *111*(E9), E09S08. <https://doi.org/10.1029/2006JE002695>
- Fedorova, A., Montmessin, F., Korablev, O., Lefèvre, F., Trokhimovskiy, A., & Bertaux, J.-L. (2021). Multi-Annual monitoring of the water vapor vertical distribution on Mars by SPICAM on Mars express. *Journal of Geophysical Research: Planets*, *126*(1), e06616. <https://doi.org/10.1029/2020JE006616>
- Fedorova, A., Rodin, A. V., & Baklanova, I. V. (2004). MAWD observations revisited: Seasonal behavior of water vapor in the Martian atmosphere. *Icarus*, *171*(1), 54–67. <https://doi.org/10.1016/j.icarus.2004.04.017>
- Fischer, E., Martínez, G. M., Rennó, N. O., Tamppari, J. K., & Zent, A. P. (2019). Relative humidity on Mars: New results from the Phoenix TECP sensor. *Journal of Geophysical Research: Planets*, *124*(11), 2780–2792. <https://doi.org/10.1029/2019JE006080>
- Fouchet, T., Lellouch, E., Ignatiev, N. I., Forget, F., Titov, D. V., Tschimmel, M., et al. (2007). Martian water vapor: Mars express PFS/LW observations. *Icarus*, *190*(1), 32–49. <https://doi.org/10.1016/j.icarus.2007.03.003>
- Gomez-Elvira, J. (2013). Mars Science Laboratory rover environmental monitoring station edr data v1.0 [Dataset]. NASA. <https://doi.org/10.17189/1523032>
- Gómez-Elvira, J., Armiens, C., Castañer, L., Domínguez, M., Genzer, M., Gómez, F., et al. (2012). REMS: The environmental sensor suite for the Mars Science Laboratory rover. *Space Science Reviews*, *170*(1–4), 583–640. <https://doi.org/10.1007/s11214-012-9921-1>
- Harri, A. M., Genzer, M., Kemppinen, O., Gomez-Elvira, J., Haberle, R., Polkko, J., et al. (2014). Mars Science Laboratory relative humidity observations: Initial results. *Journal of Geophysical Research: Planets*, *119*(9), 2132–2147. <https://doi.org/10.1002/2013JE004514>
- Heavens, N. G., Kleinböhl, A., Chaffin, M. S., Halekas, J. S., Kass, D. M., Hayne, P. O., et al. (2018). Hydrogen escape from Mars enhanced by deep convection in dust storms. *Nature Astronomy*, *2*, 126–132. <https://doi.org/10.1038/s41550-017-0353-4>
- Hietala, M., Genzer, M., Polkko, J., Jaakonaho, I., Tabandeh, S., Lorek, A., et al. (2022). MEDA HS: Relative humidity sensor for the Mars 2020 Perseverance rover. *Planetary and Space Science*, *223*, 105590. <https://doi.org/10.1016/j.pss.2022.105590>
- Imre Friedmann, E. (1982). Endolithic microorganisms in the Antarctic cold desert. *Science*, *215*(4536), 1045–1053. <https://doi.org/10.1126/science.215.4536.1045>
- Jakosky, B. M. (1985). The seasonal cycle of water on Mars. *Space Science Reviews*, *41*(1–2), 131–200. <https://doi.org/10.1007/BF00241348>
- Jakosky, B. M., & Farmer, C. B. (1982). The seasonal and global behavior of water vapor in the Mars atmosphere—Complete global results of the Viking atmospheric water detector experiment. *Journal of Geophysical Research*, *87*(B4), 2999–3019. <https://doi.org/10.1029/JB087iB04p02999>
- Jakosky, B. M., & Haberle, R. M. (1992). In M. George (Ed.), *The seasonal behavior of water on Mars* (pp. 969–1016).
- Jakosky, B. M., Zent, A. P., & Zurek, R. W. (1997). The Mars water cycle: Determining the role of exchange with the regolith. *Icarus*, *130*(1), 87–95. <https://doi.org/10.1006/icar.1997.5799>
- JCGM. (2008). Evaluation of measurement data Guide to the expression of uncertainty in measurement, JCGM 100:2008 [Computer software manual]. 92312. (Retrieved from <https://www.bipm.org/en/publications/guides>)
- Lemmon, M. T., Smith, M. D., Viudez-Moreiras, D., de la Torre-Juarez, M., Vicente-Retortillo, A., Munguira, A., et al. (2022). Dust, sand, and winds within an active martian storm in Jezero Crater. *Geophysical Research Letters*, *49*(17), e00126. <https://doi.org/10.1029/2022GL100126>
- Maltagliati, L., Montmessin, F., Fedorova, A., Korablev, O., Forget, F., & Bertaux, J. L. (2011). Evidence of water vapor in excess of saturation in the atmosphere of Mars. *Science*, *333*(6051), 1868–1871. <https://doi.org/10.1126/science.1207957>
- Mangold, N., Gupta, S., Gasnault, O., Dromart, G., Tarnas, J. D., Sholes, S. F., et al. (2021). Perseverance rover reveals an ancient delta-lake system and flood deposits at Jezero crater, Mars. *Science*, *374*(6568), 711–717. <https://doi.org/10.1126/science.aba14051>
- Martínez, G. M., Sebastián, E., Vicente-Retortillo, A., Smith, M. D., Johnson, J. R., Fischer, E., et al. (2023). Surface energy budget, albedo and thermal inertia at Jezero Crater, Mars, as observed from the Mars 2020 MEDA instrument. *Journal of Geophysical Research: Planets*, *128*, e2022JE007537. <https://doi.org/10.1029/2022JE007537>

- Martínez, G. M., Fischer, E., Rennó, N. O., Sebastián, E., Kempainen, O., Bridges, N., et al. (2016). Likely frost events at Gale crater: Analysis from MSL/REMS measurements. *Icarus*, 280, 93–102. <https://doi.org/10.1016/j.icarus.2015.12.004>
- Martínez, G. M., Newman, C. N., De Vicente-Retortillo, A., Fischer, E., Renno, N. O., Richardson, M. I., et al. (2017). The modern near-surface martian climate: A review of in-situ meteorological data from Viking to curiosity. *Space Science Reviews*, 212(1–2), 295–338. <https://doi.org/10.1007/s11214-017-0360-x>
- Martín-Torres, F. J., Zorzano, M.-P., Valentín-Serrano, P., Harri, A.-M., Genzer, M., Kempainen, O., et al. (2015). Transient liquid water and water activity at Gale crater on Mars. *Nature Geoscience*, 8(5), 357–361. <https://doi.org/10.1038/ngeo2412>
- McConnochie, T. H., Smith, M. D., Wolff, M. J., Bender, S., Lemmon, M., Wiens, R. C., et al. (2018). Retrieval of water vapor column abundance and aerosol properties from ChemCam passive sky spectroscopy. *Icarus*, 307, 294–326. <https://doi.org/10.1016/j.icarus.2017.10.043>
- Melchiorri, R., Encrenaz, T., Drossart, P., Fouchet, T., Forget, F., Titov, D., et al. (2009). OMEGA/Mars Express: South Pole Region, water vapor daily variability. *Icarus*, 201(1), 102–112. <https://doi.org/10.1016/j.icarus.2008.12.018>
- Milton, D. J. (1973). Water and processes of degradation in the Martian landscape. *Journal of Geophysical Research*, 78(20), 4037–4047. <https://doi.org/10.1029/JB078i020p04037>
- Morris, R. V., Klingelhöfer, G., Schröder, C., Rodionov, D. S., Yen, A., Ming, D. W., et al. (2006). Mössbauer mineralogy of rock, soil, and dust at Meridiani Planum, Mars: Opportunity's journey across sulfate-rich outcrop, basaltic sand and dust, and hematite lag deposits. *Journal of Geophysical Research (Planets)*, 111(E12), E12S15. <https://doi.org/10.1029/2006JE002791>
- Munigua, A., Hueso, R., Sánchez-Lavega, A., de la Torre-Juarez, M., Martínez, G. M., Newman, C. E., et al. (2023). Near surface atmospheric temperatures at Jezero from Mars 2020 MEDA measurements. *Journal of Geophysical Research: Planets*, 128, e2022JE007559. <https://doi.org/10.1029/2022JE007559>
- Navarro-González, R., Rainey, F. A., Molina, P., Bagaley, D. R., Hollen, B. J., de la Rosa, J., et al. (2003). Mars-like soils in the Atacama Desert, Chile, and the dry limit of microbial life. *Science*, 302(5647), 1018–1021. <https://doi.org/10.1126/science.1089143>
- Pla-García, J., Rafkin, S. C. R., Martínez, G. M., Vicente-Retortillo, Á., Newman, C. E., Savijärvi, H., et al. (2020). Meteorological predictions for Mars 2020 perseverance rover landing site at Jezero Crater. *Space Science Reviews*, 216(8), 148. <https://doi.org/10.1007/s11214-020-00763-x>
- Polkko, J. (2022). Data for the manuscript “initial results of the relative humidity observations by meda instrument onboard the mMars2020 perseverance rover” submitted to JGR planets m2020 special issue “crater floor” [dataset]. FMI. <https://doi.org/10.23728/fmi-b2share.daab03d71fc94bcd893b6c97adce497f>
- Rodríguez-Manfredi, J. A., & de la Torre Juárez, M. (2021). Mars 2020 MEDA bundle [dataset]. NASA. <https://doi.org/10.17189/1522849>
- Rodríguez-Manfredi, J. A., de la Torre Juárez, M., Alonso, A., Apéstigue, V., Arruego, I., Ateienza, T., et al. (2021). The Mars environmental dynamics analyzer, MEDA. A suite of environmental sensors for the Mars 2020 mission. *Space Science Reviews*, 217(3), 48. <https://doi.org/10.1007/s11214-021-00816-9>
- Savijärvi, H. I., & Harri, A. M. (2021). Water vapor adsorption on Mars. *Icarus*, 357, 114270. <https://doi.org/10.1016/j.icarus.2020.114270>
- Savijärvi, H. I., Harri, A. M., & Kempainen, O. (2015). Mars Science Laboratory diurnal moisture observations and column simulations. *Journal of Geophysical Research (Planets)*, 120(5), 1011–1021. <https://doi.org/10.1002/2014JE004732>
- Savijärvi, H. I., Harri, A.-M., & Kempainen, O. (2016). The diurnal water cycle at Curiosity: Role of exchange with the regolith. *Icarus*, 265, 63–69. <https://doi.org/10.1016/j.icarus.2015.10.008>
- Savijärvi, H. I., Martínez, G., Harri, A.-M., & Paton, M. (2020a). Curiosity observations and column model integrations for a Martian global dust event. *Icarus*, 337, 113515. <https://doi.org/10.1016/j.icarus.2019.113515>
- Savijärvi, H. I., Martínez, G. M., Fischer, E., Renno, N. O., Tamppari, L. K., Zent, A., & Harri, A. M. (2020b). Humidity observations and column simulations for a warm period at the Mars Phoenix lander site: Constraining the adsorptive properties of regolith. *Icarus*, 343, 113688. <https://doi.org/10.1016/j.icarus.2020.113688>
- Savijärvi, H. I., Martínez, G. M., Vicente-Retortillo, A., & Harri, A. M. (2022). Surface energy budget at Curiosity through observations and column modeling. *Icarus*, 376, 114900. <https://doi.org/10.1016/j.icarus.2022.114900>
- Savijärvi, H. I., McConnochie, T. H., Harri, A.-M., & Paton, M. (2019). Water vapor mixing ratios and air temperatures for three Martian years from Curiosity. *Icarus*, 326, 170–175. <https://doi.org/10.1016/j.icarus.2019.03.020>
- Savijärvi, H. I., & Silli, T. (1993). The Martian slope winds and the nocturnal PBL jet. *Journal of the Atmospheric Sciences*, 50(1), 77–88. [https://doi.org/10.1175/1520-0469\(1993\)050<0077:TMSWAT>2.0.CO;2](https://doi.org/10.1175/1520-0469(1993)050<0077:TMSWAT>2.0.CO;2)
- Sebastián, E., Martínez, G., Ramos, M., Pérez-Grande, I., Sobrado, J., & Rodríguez Manfredi, J. A. (2021). Thermal calibration of the MEDA-TIRS radiometer onboard NASA's Perseverance rover. *Acta Astronautica*, 182, 144–159. <https://doi.org/10.1016/j.actastro.2021.02.006>
- Sindoni, G., Formisano, V., & Geminala, A. (2011). Observations of water vapour and carbon monoxide in the Martian atmosphere with the SWC of PFS/MEX. *Planetary and Space Science*, 59(2–3), 149–162. <https://doi.org/10.1016/j.pss.2010.12.006>
- Smith, D. E., Zuber, M. T., Solomon, S. C., Phillips, R. J., Head, J. W., Garvin, J. B., et al. (1999). The global topography of Mars and implications for surface evolution. *Science*, 284(5419), 1495–1503. <https://doi.org/10.1126/science.284.5419.1495>
- Smith, M. D. (2002). The annual cycle of water vapor on Mars as observed by the Thermal Emission Spectrometer. *Journal of Geophysical Research: Planets*, 107(E11), 5115–5125-19. <https://doi.org/10.1029/2001JE001522>
- Smith, M. D. (2004). Interannual variability in TES atmospheric observations of Mars during 1999–2003. *Icarus*, 167(1), 148–165. <https://doi.org/10.1016/j.icarus.2003.09.010>
- Smith, M. D., Daerden, F., Neary, L., & Khayat, A. (2018). The climatology of carbon monoxide and water vapor on Mars as observed by CRISM and modeled by the GEM-Mars general circulation model. *Icarus*, 301, 117–131. <https://doi.org/10.1016/j.icarus.2017.09.027>
- Smith, M. D., Pearl, J. C., Conrath, B. J., & Christensen, P. R. (2001). Thermal emission spectrometer results: Mars atmospheric thermal structure and aerosol distribution. *Journal of Geophysical Research*, 106(E10), 23929–23945. <https://doi.org/10.1029/2000JE001321>
- Smith, M. D., Wolff, M. J., Clancy, R. T., & Murchie, S. L. (2009). Compact Reconnaissance Imaging Spectrometer observations of water vapor and carbon monoxide. *Journal of Geophysical Research: Planets*, 114(E9), E00D03. <https://doi.org/10.1029/2008JE003288>
- Smith, P. H., Tamppari, L. K., Arvidson, R. E., Bass, D., Blaney, D., Boynton, W. V., et al. (2009). H₂O at the Phoenix landing site. *Science*, 325(5936), 58–61. <https://doi.org/10.1126/science.1172339>
- Spinrad, H., Münch, G., & Kaplan, L. D. (1963). Letter to the editor: The detection of water vapor on Mars. *The Astrophysical Journal*, 137, 1319. <https://doi.org/10.1086/147613>
- Sprague, A. L., Hunten, D. M., Doose, L. R., & Hill, R. E. (2003). Mars atmospheric water vapor abundance: 1996–1997. *Icarus*, 163(1), 88–101. [https://doi.org/10.1016/S0019-1035\(03\)00072-1](https://doi.org/10.1016/S0019-1035(03)00072-1)
- Sprague, A. L., Hunten, D. M., Hill, R. E., Rizk, B., & Wells, W. K. (1996). Martian water vapor, 1988–1995. *Journal of Geophysical Research*, 101(E10), 23229–23254. <https://doi.org/10.1029/96JE02265>
- Steele, L. J., Balme, M. R., Lewis, S. R., & Spiga, A. (2017). The water cycle and regolith-atmosphere interaction at Gale crater, Mars. *Icarus*, 289, 56–79. <https://doi.org/10.1016/j.icarus.2017.02.010>

- Tamppari, L. K., & Lemmon, M. T. (2020). Near-surface atmospheric water vapor enhancement at the Mars Phoenix lander site. *Icarus*, 343, 113624. <https://doi.org/10.1016/j.icarus.2020.113624>
- Vaisala-Oyj (2020). Humicap technology description (Tech. Rep. No. B210781EN-D). Retrieved from <https://www.vaisala.com/sites/default/files/documents/HUMICAP-Technology-description-B210781EN.pdf>
- Viúdez-Moreiras, D., de la Torre, M., Gómez-Elvira, J., Lorenz, R., Apéstitigue, V., Guzewich, S., et al. (2022). Winds at the Mars 2020 landing site. part 2: Wind variability and turbulence. *Journal of Geophysical Research: Planets*, 127(12), e2022JE007523. <https://doi.org/10.1029/2022JE007523>
- Viúdez-Moreiras, D., Lemmon, M., Newman, C., Guzewich, S., Mischna, M., Gómez-Elvira, J., et al. (2022). Winds at the Mars 2020 landing site: 1. Near-surface wind patterns at Jezero Crater. *Journal of Geophysical Research: Planets*, 127(12), e2022JE007522. <https://doi.org/10.1029/2022JE007522>
- Viúdez-Moreiras, D., Newman, C. E., de la Torre, M., Martínez, G., Guzewich, S., Lemmon, M., et al. (2019). Effects of the MY34/2018 global dust storm as measured by MSL REMS in Gale Crater. *Journal of Geophysical Research: Planets*, 124(7), 1899–1912. <https://doi.org/10.1029/2019JE005985>
- VTT-Ltd. (2022). *Uncertainty evaluation of meda hs humidity measurements* (Tech. Rep.). (“State Research Center (VTT) consultation report with Finnish Meteorological Institute, 2022 by Tabandeh, S. and Högstrom, R.”)
- Whiteway, J. A., Komguem, L., Dickinson, C., Cook, C., Illnicki, M., Seabrook, J., et al. (2009). Mars water-ice clouds and precipitation. *Science*, 325(5936), 68–70. <https://doi.org/10.1126/science.1172344>
- Young, I., Crawford, J., Nunan, N., Otten, W., & Spiers, A. (2008). *Chapter 4 microbial distribution in soils: Physics and scaling*. In (Vol. 100, p. 81–121). Academic Press. [https://doi.org/10.1016/S0065-2113\(08\)00604-4](https://doi.org/10.1016/S0065-2113(08)00604-4)
- Zent, A. P., Hecht, M. H., Cobos, D. R., Wood, S. E., Hudson, T. L., Milkovich, S. M., et al. (2010). Initial results from the thermal and electrical conductivity probe (TECP) on Phoenix. *Journal of Geophysical Research*, 115(2), E00E14. <https://doi.org/10.1029/2009JE003420>
- Zent, A. P., Hecht, M. H., Hudson, T. L., Wood, S. E., & Chevrier, V. F. (2016). A revised calibration function and results for the Phoenix mission TECP relative humidity sensor. *Journal of Geophysical Research: Planets*, 121(4), 626–651. <https://doi.org/10.1002/2015JE004933>